

January 2022

Application Of Gravity Data For Hydrocarbon Exploration Using Machine Learning Assisted Workflow

Oluwafemi Temidayo Alaofin

Louisiana State University and Agricultural and Mechanical College

Follow this and additional works at: https://digitalcommons.lsu.edu/gradschool_theses



Part of the [Artificial Intelligence and Robotics Commons](#), [Data Science Commons](#), [Environmental Health and Protection Commons](#), [Geology Commons](#), [Geophysics and Seismology Commons](#), [Natural Resources and Conservation Commons](#), [Oil, Gas, and Energy Commons](#), and the [Petroleum Engineering Commons](#)

Recommended Citation

Alaofin, Oluwafemi Temidayo, "Application Of Gravity Data For Hydrocarbon Exploration Using Machine Learning Assisted Workflow" (2022). *LSU Master's Theses*. 5482.

https://digitalcommons.lsu.edu/gradschool_theses/5482

This Thesis is brought to you for free and open access by the Graduate School at LSU Digital Commons. It has been accepted for inclusion in LSU Master's Theses by an authorized graduate school editor of LSU Digital Commons. For more information, please contact gradetd@lsu.edu.

APPLICATION OF GRAVITY DATA FOR HYDROCARBON EXPLORATION USING MACHINE LEARNING ASSISTED WORKFLOW

A Thesis

Submitted to the Graduate Faculty of the
Louisiana State University and
Agricultural and Mechanical College
in partial fulfillment of the
requirements for the degree of
Master of Science

in

The Craft & Hawkins Department of Petroleum Engineering

by

Oluwafemi Temidayo Alaofin

B.Tech., Ladoke Akintola University of Technology, Nigeria, 2015

M.Sc., Offshore Technology Institute, Nigeria, 2018

May 2022

To my father and mother, Joseph, and Oluyemisi Alaofin, they taught me to always work hard
and believe in God.

To my brother, Olakunle Alaofin who has always there when I needed someone to talk to.

ACKNOWLEDGMENTS

I would like to specially thank my advisor, Dr. Jyotsna Sharma, for her advice and support throughout this journey. I would also like to thank the other members of my committee members, Dr. Mayank Tyagi and Dr. Xin (Shane) Li for their time and assistance throughout this process. I would like to express my gratitude to Dr. Jian Zhang, my minor professor in computer science, and Yi Zhang, a member of my research group, who have been extremely helpful and supportive during my time at LSU. Finally, I would like to express my gratitude to my parents for their unwavering support and guidance over the years. Kunle, my brother, was always there for me through thick and thin. I will be eternally grateful for his attentive ears and encouraging words.

TABLE OF CONTENTS

ACKNOWLEDGMENTS	iii
LIST OF TABLES	v
LIST OF FIGURES	i
ABSTRACT.....	i
Chapter 1. INTRODUCTION	1
1.2. Challenges with using Seismic Data	2
1.3. Gravimetry.....	3
1.4. Problem Statements and Objectives	4
1.5. Thesis Organization	6
Chapter 2. LITERATURE REVIEW	7
2.1. Gravity Survey	7
2.2. Gravity Anomalies	8
2.3. Random Forest Algorithm	13
Chapter 3. METHODOLOGY	16
3.1. Research Methodology Workflow.....	16
3.2. Data Collection, Preparation, and Processing	18
3.3. Classification Accuracy Assessment	23
Chapter 4. RESULTS	25
4.1. Land-based Gravity Anomaly Prediction	25
4.2. Satellite-based Gravity Anomaly Prediction Results	41
4.3. Enhanced Satellite-based Bouguer Gravity Prediction Results	48
Chapter 5. CONCLUSION	56
Chapter 6. RECOMMENDATIONS.....	57
BIBLIOGRAPHY	58
VITA.....	63

LIST OF TABLES

2.1. List of geophysical methods and their characteristics (Kearey & Brooks, 1991)	8
4.1. Range of input features	26
4.2. Number of data points in the different classes	26
4.3. Random Forest regression results for Bouguer land-based gravity prediction.....	26
4.4. Random Forest regression results for isostatic gravity prediction.....	27
4.5. Random Forest hydrocarbon classification train dataset report.....	30
4.6. Random Forest hydrocarbon classification validation dataset report	30
4.7. Random Forest hydrocarbon classification test dataset report	30
4.8. Hydrocarbon classification confusion matrix for test dataset.....	31
4.9. Petrel hydrocarbon classification testing dataset report.....	32
4.10. Land-based hydrocarbons vs no hydrocarbons classification training results.....	35
4.11. Land-based hydrocarbons vs no hydrocarbons classification testing results.....	36
4.12. Land-based oil vs no oil classification training results	37
4.13. Land-based oil vs no oil classification testing results.....	38
4.14. Land-based gas vs no gas classification training results.....	39
4.15. Land-based gas vs no gas classification training results.....	40
4.16. Range of input features	41
4.17. Random Forest regression results for satellite based Bouguer gravity prediction.....	42

4.18. Random Forest hydrocarbons classification training dataset report	43
4.19. Random Forest hydrocarbon classification validation dataset report	43
4.20. Random Forest hydrocarbon classification test dataset report	44
4.21. Hydrocarbon classification confusion matrix for test dataset.....	44
4.22. Petrel hydrocarbon classification testing dataset report.....	45
4.23. Satellite-based hydrocarbons vs no hydrocarbons classification results	47
4.24. Satellite-based oil vs no oil classification results	47
4.25. Satellite-based gas vs no gas classification results	48
4.26. Range of input features	49
4.27. Random Forest regression results for Bouguer gravity prediction	49
4.28. Random Forest regression results for free-air gravity prediction	50
4.29. Random Forest hydrocarbon classification training dataset report.....	51
4.30. Random Forest hydrocarbon classification validation dataset report	51
4.31. Random Forest hydrocarbon classification testing report	52
4.32. Classification confusion matrix for test dataset	52
4.33. Petrel hydrocarbon classification testing dataset report.....	53
4.34. Super resolution satellite-based hydrocarbons vs no hydrocarbons classification results...	54
4.35. Super resolution satellite-based oil vs no oil classification training results	54
4.36. Super resolution satellite-based gas vs no gas classification training results	55

LIST OF FIGURES

1.1. Sketch of the SRCNN architecture (Zhang, Yi et al., 2021).....	4
1.2. Hydrocarbon Classification Workflow utilizing the Random Forest algorithm and Schlumberger Petrel E & P Software Platform (v. 2020).....	5
2.1. Free-air and Bouguer anomalies across a mountain range (Lowrie, 1997)	11
3.1. Workflow for hydrocarbon exploration classification using machine learning.....	17
3.2. Detailed oil and gas field map used in the model (Source: US EIA).	19
3.3. Visual representation of regions (well locations) used for the hydrocarbon classification algorithm.	20
3.4. US land based Bouguer gravity anomaly map (in mgals).	21
3.5. US satellite based Bouguer gravity anomaly map (in mgals).....	22
3.6. Enhanced US satellite based Bouguer gravity anomaly map (in mgals) using super-resolution algorithm (Zhang Yi et al., 2021).	22
4.1. (a) Bouguer gravity anomaly map for the United States (b) Section chosen for interpolation (c) A zoomed-in section of the Bouguer gravity data points (d) Interpolated Bouguer gravity data points filled in with geospatial trend.....	27
4.2. Convergent interpolated Bouguer gravity points within polygon field.	28
4.3. Isostatic gravity Random Forest classification model feature importance	31
4.4. Random Forest classification model features importance	32
4.5. Petrel hydrocarbon classification model features importance	33
4.6. Random Forest hydrocarbon classification model features importance	44
4.7. Petrel hydrocarbon classification model features importance	45
4.8. Random Forest classification model feature importance.....	52
4.9. Petrel hydrocarbon classification model features importance	53

ABSTRACT

Gravity survey has played an essential role in many geoscience fields ever since it was conducted, especially as an early screening tool for subsurface hydrocarbon exploration. With continued improvement in data processing techniques and gravity survey accuracy, in-depth gravity anomaly studies, such as characterization of Bouguer and isostatic residual anomalies, have the potential to delineate prolific regional structures and hydrocarbon basins. In this study, we focus on developing a cost-effective, quick, and computationally efficient screening tool for hydrocarbon exploration using gravity data employing machine learning techniques. Since land-based gravity surveys are often expensive and difficult to obtain in remote places, we explore the use of satellite-based gravity, which is available throughout the Earth and updated periodically. Since the accuracy and resolution of the satellite gravity data are lower than land-based gravity measurement, satellite data was enhanced through a deep-learning-based super-resolution technique. We compare the use of land-based, satellite-based, and enhanced-satellite Bouguer and isostatic gravity data for the classification of hydrocarbon regions using both supervised and unsupervised machine learning techniques. In addition, a comparison of geostatistical models and Random Forest regression is performed for geospatial interpolation. The use of different combinations of input features (Bouguer, isostatic gravity, latitude, longitude coordinates) and prediction classes (oil, gas, oil and gas, no hydrocarbons) are evaluated and compared. Results indicate the successful application of supervised machine learning workflow for hydrocarbon classification using Bouguer and isostatic gravity anomalies with good prediction accuracy for both land-based and satellite-based gravity data. The results from unsupervised machine learning were less robust in comparison.

Chapter 1. INTRODUCTION

Hydrocarbon exploration involves searching for undiscovered oil and gas resources with the purpose of obtaining a successful and profitable oil and gas extraction (Adelman, 1970). It is a costly, high-risk operation that necessitates a thorough understanding of the geological context and operational challenges, from discovery to reserve estimation, and finally moving the reserves to production (Melay et al., 2003). The current exploration model for the oil and gas industry forces it to go through a lengthy and arduous process before reaching conclusions about the prospect potential of those regions. The process of identifying potential areas and risk reduction assessments prior to drilling the first exploratory well can take years and requires investments that the industry cannot currently justify. Many potentially attractive areas are left unexplored for long periods of time due to the cost, time, and risk involved in such exploratory campaigns. A new exploration model should enable a faster, less expensive, and more direct method of assessing the prospect of large exploratory areas and identifying oil and gas leads. New and emerging technologies will be critical to achieving this change. The gravity survey method is one of the earliest techniques used in oil and gas exploration. Despite the introduction of seismology, it has remained an important early screening step in hydrocarbon subsurface mapping and exploration. Land-based and airborne (including satellite-based) surveys are the two most common methods for obtaining gravity data. For local/regional surveys, land-based gravity data is commonly used. They can, however, be difficult to obtain economically for large-scale area prospects and remote locations. The satellite-based gravity survey can be used for regional studies as a faster and less expensive alternative method to ground measurement (Yanis & Marwan, 2019a; M. hua Zhang et al., 2019).

With improved data processing technology and gravity survey accuracy, in-depth gravity anomaly studies, such as characterization of Bouguer anomalies and isostatic residual anomalies,

have become critical in the delineation and tracking of prolific regional and trap structures within potential hydrocarbon basins (L. Liu et al., 2018; M. H. Zhang et al., 2013). Gravity anomaly differences and characteristics between basins reflect variations in crustal thickness, basement properties, depth, stratigraphic framework, and overlying cover strata structures (Aghajani et al., 2011; Berezkin, n.d.; Dung, 2004; McCulloh, 1967; Yanis & Marwan, 2019b). However, there has been very limited research into using gravity data with machine learning applications as an early screening step to select potential oil and gas fields. To this end, this research investigates the use of the Random Forest ensemble machine learning method for modeling and training gravity data to provide a quick and cost-effective approach in the early screening of high-potential oil and gas fields during the early stages of hydrocarbon exploration.

1.2. Challenges with using Seismic Data

Seismic surveying is a technique used in the exploration phase of oil and gas development. The method provides a preliminary understanding of what lies beneath the earth's surface. Energy generated by instruments such as a seismic vibrator (on land) or an air gun (in water) creates seismic waves that travel through the earth's layers and "bounce back" from different rock layers. The seismic waves that are reflected and refracted are recorded by a receiver (geophones or hydrophones in water) and provide the first image of the subsurface. This technique allows for the interpretation of what is beneath the ground or seabed (oil, gas, water, faults, folds, and so on) without the need to drill. However, seismic surveys, are very expensive, with data processing taking time and requiring highly specialized expertise. It also poses environmental challenges and could potentially endanger marine life. Compared to the gravity surveys, the use of seismic data results in a higher carbon footprint (CO₂ emissions from marine seismic surveys). One of the biggest advantages of using gravity surveys for exploration is our ability to get them periodically

from satellites. This is especially advantageous for exploration in remote locations where land-based surveys are difficult to conduct, while satellite data is readily available throughout the world.

1.3. Gravimetry

Gravimetry is a vital geophysical exploration technique that makes use of local changes in acceleration due to gravity caused by the non-uniform density distribution of crustal materials. Precision gyro-stabilized gravimeters can be used to measure gravity from the ground. (Sokolov, 2011). Land-based gravity measurements, on the other hand, can be difficult in remote areas such as mountains, bogs, sea-and-land boundary areas, and the Earth's polar caps. Measuring gravity from a satellite (or satellite gravimetry) is a new geophysical method that is very promising for large-scale exploration (Crowley et al., 2006; Kern et al., 2003). Its main advantage is that it makes geophysical studies of remote regions possible. However, when compared to ground-based gravity measurements, satellite-based gravity measurements have a lower resolution and precision. To address this, deep learning technique of image super-resolution (SR) based on deep learning has been utilized in this study to estimate the high-resolution (HR) counterpart x of a given low-resolution (LR) image y , through training with high-resolution data (Baker & Kanade, 2002). The basic principle of super resolution is to use one low-resolution image or a sequence of low-resolution images of a scene to create an image with higher spatial resolution that contains finer detail or content with higher frequencies than the low-resolution images. Super-resolution can be used to improve the low spatial resolution and precision of satellite-based gravity data to the level of ground gravity data, which provides more information. Figure 1.1 shows super-resolution (SRCNN) architecture proposed by (Dong et al., 2014) and (2015), which was the pioneering work of using a convolutional neural network in image super-resolution reconstruction development. It utilizes three convolutional layers to predict the HR image.

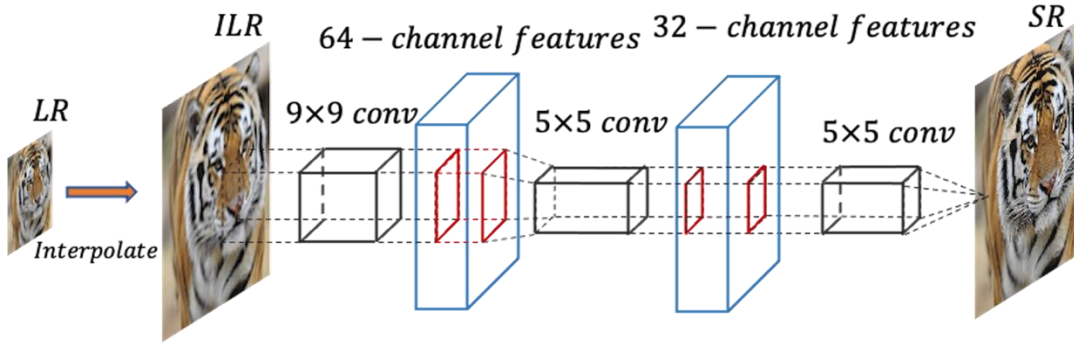


Figure 1.1. Sketch of the SRCNN architecture (Zhang, Yi et al., 2021).

1.4. Problem Statements and Objectives

The overall objective of this research is to advance the development of a cost-effective, quick, and computationally efficient screening tool for hydrocarbon exploration using gravity data employing machine learning techniques. The following are a set of partial objectives:

1. Application of machine learning techniques for geospatial interpolation and hydrocarbon exploration.
2. Comparison of geostatistical models and Random Forest regression methods for geospatial interpolation.
3. Identification and optimization of the machine learning model's most important features and predictors.
4. Evaluation of the effectiveness of the Random Forest classifier for hydrocarbon exploration using land-based gravity data.
5. Evaluation of the effectiveness of the Random Forest classifier for hydrocarbons using satellite-based low-resolution gravity data and satellite data whose resolution has been improved using super-resolution techniques.

The above objectives have been addressed through the following tasks:

a. **Data collection for oil and gas reserves and gravity anomalies:**

- (1) Hydrocarbon field information, wells data and their geographic coordinates.
- (2) Gravity anomalies, including Bouguer and isostatic gravity, from land-based surveys.

b. **Data analysis:**

- (1) Random Forest and geospatial kriging techniques for gravity interpolation.
- (2) Random Forest classification of hydrocarbon deposits.

c. **Results analysis:**

Compare different modeling approaches, feature selection, and results to assess the performance of various models in accurately identifying hydrocarbon deposits.

The above research approach can be summarized through the schematic presented in Figure 1.2.

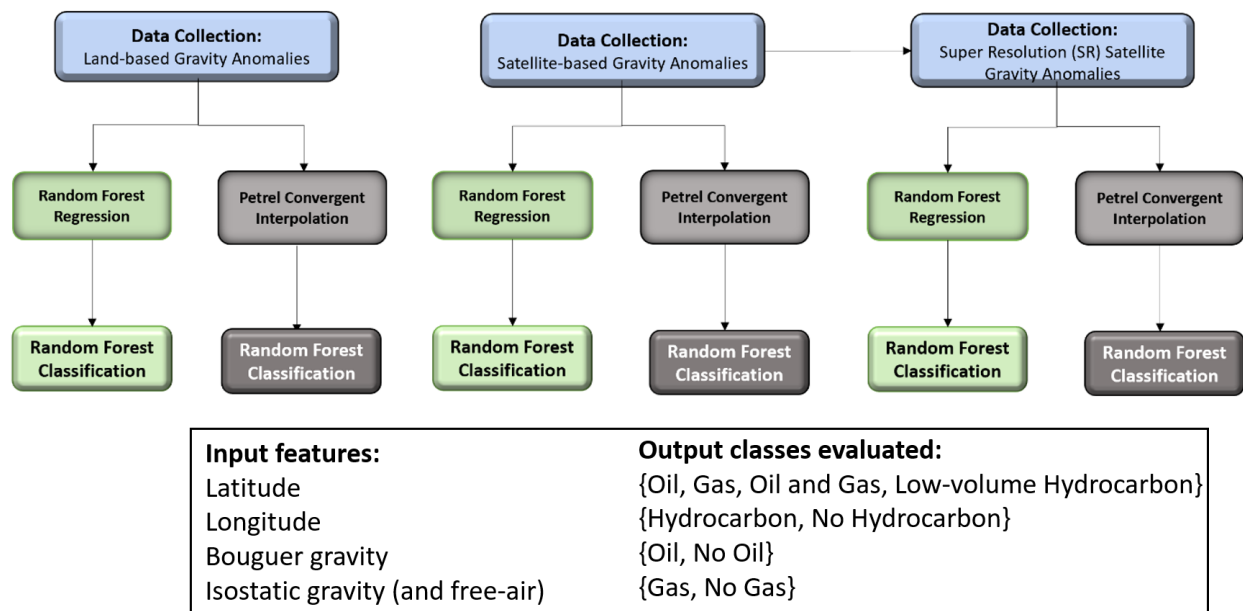


Figure 1.2. Hydrocarbon Classification Workflow utilizing the Random Forest algorithm and Schlumberger Petrel E & P Software Platform (v. 2020)

1.5. Thesis Organization

The first chapter of this thesis explains why gravity data is important in hydrocarbon exploration and the processes involved in acquiring them. The second chapter delves into the various gravity properties and the models that have been used to characterize the process. The research workflow process and its assessment metrics are discussed in Chapter 3, and the results for the investigated parameters are presented in Chapter 4. The significant findings of this investigation, as well as recommendations for future work, are presented in Chapter 5.

Chapter 2. LITERATURE REVIEW

2.1. Gravity Survey

In the early stages of exploration, geophysical methods are the most effective and successful for targeting prolific basins and delineating the boundaries of concealed and partially concealed basins and main structures within the basins. Magnetic, gravity and seismic surveys are the three main geophysical methods used in hydrocarbon exploration. Magnetic and gravity surveys are typically used prior to drilling, whereas seismic surveys are used for exploration and development. The seismic method is the most commonly used method for investigating subsurface structures. However, within salt provinces, the seismic quality deteriorates, and in this case, the gravity survey becomes more suitable. Seismic data is also costly to acquire, especially in offshore environments. Various studies show that successful gravity data applications in hydrocarbon exploration (G. Liu et al., 2020; Sarsar Naouali et al., 2017; Yanis & Marwan, 2019b; M. hua Zhang et al., 2019). The gravity survey method measures the Earth's gravitational field at specific locations, revealing variations in subsurface lateral density. It is primarily used in basement structural mapping of sedimentary basins (De Castro D L and Bezerra F H R, 2011). Chen et al., (2020) used an innovative method of machine learning based on a U-net deep neural network to determine salt structures directly from gravity data. Subsurface structures have different masses because they have a higher or lower density than the surrounding materials. The measured gravity data is influenced by the shape and rotation of the Earth, as well as tides and the Earth itself. Before delineating subsurface features, gravity data anomalies, which describe the local variations of the gravity field around the model field, must be corrected by removing these attributed factors (McLean et al., 2009). Table 2.1 depicts the various types of geophysical surveying methods, as well as the physical properties that are most sensitive to measure.

Table 2.1. List of geophysical methods and their characteristics (Kearey & Brooks, 1991)

Method	Measured parameter	Operative physical property
Seismic	Travel times of reflected/refracted seismic waves	Density and elastic moduli determine the propagation velocity of seismic waves
Gravity	Spatial variations in the strength of the gravitational field of the Earth	Density
Magnetic	Spatial variations in the strength of the geomagnetic field	Magnetic susceptibility and remanence
Electric Resistivity	Earth resistance	Electrical conductivity
Induced polarization	Polarization voltages or frequency-dependent ground resistance	Electrical capacitance
Self-potential	Electrical potentials	Electrical conductivity
Electromagnetic	Response to electromagnetic radiation	Electrical conductivity and inductance
Radar	Travel times of reflected radar pulses	Dielectric constant

2.2. Gravity Anomalies

Gravity is the attraction between two bodies, and the strength of this attraction is determined by the mass of the two bodies as well as their distance apart. Gravity is measured in the unit of gals where one gal equals one centimeter per second. Gravity is not the same everywhere on Earth due to a variety of factors. Gravity surveys use these small gravity changes caused by variations in subsurface rock density to learn about the planet's internal structure. Denser rocks have higher gravity values, while less dense rocks have lower gravity (P. Hill, V. Bankey, 1997). Gravity anomalies are differences between the true gravity field of the Earth and the theoretical gravity of a reference body. In simple terms, the difference between the observed acceleration of an object in free fall on the surface of a planet and the corresponding value predicted by a model of the

planet's gravitational field (Balmino & Bonvalot, 2016). There are different types of gravity anomalies, namely free-air gravity anomalies, Bouguer gravity, and isostatic gravity anomalies.

2.2.1. Bouguer Gravity Anomaly

The Bouguer anomaly (named after Pierre Bouguer) is a gravity anomaly that has been corrected for the height at which it is measured as well as terrain attraction. A free-air gravity anomaly is produced by the height correction alone. The distinction is in the types of corrections applied to the measured gravitational acceleration at the various stations (Ervin, 1977; Karl, 1971; Takin & Talwani, 1966; Zamora, 2013). Assuming uniform subsurface density, the Earth's gravitational field would be constant everywhere after the appropriate corrections were applied. On the other hand, gravity anomalies would be any "local variation from the otherwise constant gravitational field" caused by any lateral density variations caused by changes in subsurface geology (Kearey et al., 2002).

For calculation purposes, normal gravity, g_n , is assumed to have a uniform, homogeneous, elliptical Earth as its theoretical shape (Lowrie, 1997). Using the formula, it is subtracted from the absolute gravity on the reference ellipsoid as shown in equation 2.3:

$$g_n = g_e(1 + \beta_1 \sin(\lambda)^2 + \beta_2 \sin(2\lambda)^4) \quad (2.1)$$

where $g_e = 9.780327 \frac{m}{s^2}$, $\beta_1 = 5.30244 \times 10^{-3}$, $\beta_2 = -5.8 \times 10^{-6}$, and λ = latitude

Relative gravity to a base station can be corrected by differentiating the reference formula, g_n , with respect to, λ , so that a change in distance from the base station results in a change in the gravitational attraction given by the formula based on latitude as:

$$\Delta g_{lat} = 0.814 \sin(2\lambda) \quad (2.2)$$

Δg_{lat} , mGals per kilometer of displacement in the North-South direction is deducted from stations located closer to the pole than the base station.

The terrain, Bouguer, and free-air corrections compensate for the gravity value, which is usually not on the ellipsoid. The Bouguer gravity anomaly, Δg_B is obtained by applying all of the previously described corrections:

$$\Delta g_B = g_{obs} + (\Delta g_{FA} - \Delta g_{BP} + \Delta g_T + \Delta g_{tide}) - g_n \quad (2.3)$$

Here, g_{obs} is the measured gravity value, g_n is the theoretical (or normal) gravity value, and the corrections used are free-air (Δg_{FA}), Bouguer plate (Δg_{BP}), terrain (Δg_T), and tidal (Δg_{tide}). The Free-air gravity anomaly, Δg_F , is obtained by applying only the free-air, terrain, and tidal corrections to the observed gravity:

$$\Delta g_F = g_{obs} + (\Delta g_{FA} + \Delta g_T + \Delta g_{tide}) - g_n \quad (2.4)$$

free-air anomaly, $FA = g_0 - \gamma_0 + Fe$ and Bouguer anomaly, $BA = FA - Be$

where g_0 = observed gravity; γ_0 = theoretical gravity, Fe = free-air effect, and Be = Bouguer effect. The free-air effect (Fe) is a function of the observed station's elevation or depth above or below the reference ellipsoid, which is taken here as mean sea level.

$$Fe = \left(\frac{dg}{dz} \right) h - \left(\frac{dg}{dz} - 4\pi G \rho_w \right) d_w \quad (2.5)$$

where $\frac{dg}{dz}$ is the vertical gradient of gravity equal to 0.3086 mGal/ m, h is the station elevation in meters, G the universal constant of gravitation ($6.672 \times 10^{-8} \text{ m}^3 / \text{Mgs}^2$), ρ_w the density of seawater (1.03 Mg/ m^3), and d_w the depth of water for underwater stations only. The Bouguer effect (Be) depends on whether the mass is above or below the reference ellipsoid. The usual

mass correction is a semi-infinite flat slab whose top and bottom coincide with the station and sea level, respectively.

$$Be = 2\pi G\rho_c h + 2\pi G(\rho_c - \rho_w)d_w + 2\pi G(\rho_c - \rho_i)d_i \quad (2.6)$$

where $2\pi G = 0.04192 \times 10^{-5} \text{ m}^3/\text{Mgs}^2$, ρ_c is the assumed surface crustal density ($2.67 \text{ Mg}/\text{m}^3$), ρ_i is the assumed density of ice ($0.9 \text{ Mg}/\text{m}^3$), and d_i is the thickness of ice in meters.

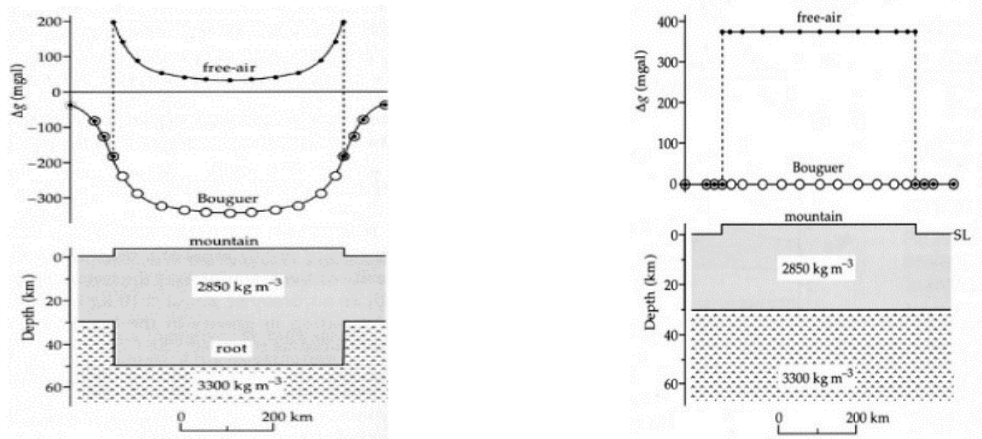


Figure 2.1. Free-air and Bouguer anomalies across a mountain range (Lowrie, 1997)

There may be an important distinction between Bouguer and free-air anomalies across the same structure, as shown in Figure 2.1, which depicts two simplified representations of a mountain range. Free-air anomalies are commonly used in geodetic applications. Bouguer anomalies, on the other hand, are used in geophysical applications because they demonstrate the effects of different subsurface rock density distributions on gravity anomaly observations (Zamora, 2013).

2.2.2. Isostatic Gravity Anomaly

Although the Bouguer reduction process eliminates the gravitational effects of altitude, latitude, and topographic mass on sea level, it does not account for compensating mass at depth. As a result, an inverse linear correlation with topography persists. To eliminate this effect and

improve the signal as a result of intra-crustal density contrasts. The Bouguer gravity field data is isostatically corrected, removing regional trends and producing a superior gravity dataset for sedimentary-basin analysis (Heywood, 1992).

The principle of isostasy states that topographic loads at the surface compensate for mass deficiencies at depth, which are also known as isostatic roots. The effects of these mass deficiencies are not considered during the Bouguer reduction process, and there is an inverse relationship between broad Bouguer anomaly lows and positive topography. The isostatic correction eliminates the isostatic roots' gravity anomaly effect. Historically, the concept arose from the observation that Bouguer anomalies in mountainous areas are always negative and have large values, with an average of 100 mGal per 1000 m of elevation. This means that topographic masses are compensated for by some mechanism. There have been two different models proposed: According to (Airy, 1855), the first model assumes that topographic masses of density ρ_c float on a denser layer (Earth's upper mantle) of density ρ_m ; thus, roots of height t exist under the continental layer and anti-roots of height t^* exist under the ocean layer. The floating equilibrium condition yields:

$$t = \frac{\rho_c}{\rho_m - \rho_c} H \quad (2.7)$$

$$t^* = \frac{\rho_c - \rho_w}{\rho_m - \rho_c} H^* \quad (2.8)$$

The second model proposed by (Pratt, 1855) assumes a level of compensation at depth D_c at constant pressure. As a result, the density of a given column of material varies and is affected by its elevation. In planar approximation, it is over continents:

$$\rho = \frac{D_c}{H-D_c} \rho_c \quad (2.9)$$

which is slightly smaller than its normal value ρ_c . While over the oceans, it is:

$$\rho^* = \rho_c + \frac{H^*}{D_c-H^*} \rho_c - \rho_w \quad (2.10)$$

Where t is the structural root height beneath the continental layer, t^* is the structural anti-root height beneath the continental layer, ρ_c is the density of topographic masses, ρ_m is the density of Earth's upper mantle, ρ_w is the density of water, D_c is the depth of compensation mass, H is the orthometric height, and H^* is the normal height. All the parameters H , H^* , t , and t^* are positive and correspond to mass surplus. Other formulas for other situations (lakes, ice caps, etc.) are available and can be found in (Balmino, G., Vales, N., Bonvalot, S., and Briais, 2012). Finally, using the adopted model, the gravitational attraction, δg_{ISO} , of the anomalous mass distribution under the topography can be computed, and the isostatic anomaly, Δg_{ISO} , is the sum of the Bouguer anomaly, Δg_B , and the isostatic correction, δg_{ISO} .

2.3. Random Forest Algorithm

The use of ensemble learning methods has increased because they can be more accurate and robust than single classifiers (Dietterich, 2000). Boosting (R. Shapire, Y. Freund, P. Bartlett, 1998) and bagging (Breiman, 1996) classification trees are two well-known methods. In boosting, successive trees give extra weight to points predicted incorrectly by previous predictors. Finally, a weighted vote is cast for prediction. While bagging, subsequent trees are not dependent on previous trees; instead, each is constructed independently using a bootstrap sample of the data set, and a simple majority vote is taken for prediction at the end. Bootstrap aggregation (bagging) is a

training technique that involves randomly resampling the original dataset with replacement data (i.e., with no deletion of the data selected from the input sample for generating the following subset). (Breiman, 2001) proposed Random Forest, which add a layer of randomness to the bagging approach, were proposed. The best split among all variables for each node is used in standard tree splitting. Each node in a Random Forest employs the best predictor from a subset of predictors chosen at random at that node. This seemingly counterintuitive strategy outperforms many other classifiers, including discriminant analysis, support vector machines, and neural networks, and is resistant to overfitting (Breiman, 2001). The Random Forest algorithm is useful for both regression and classification. Regression Random Forest is an ensemble learning method that generates many regressions tree models from bootstrap samples of training data. The model's performance is measured using the R-square (R^2) and root-mean-square error (RMSE). The R-square, also known as the coefficient of determination or, for multiple regression, the coefficient of multiple determination, is a statistical measure of how close the data are to the fitted regression line, which is mathematically expressed as:

$$R^2 = 1 - \frac{\sum(\hat{y} - \bar{y})^2}{\sum(y - \bar{y})^2} \quad (2.11)$$

The criterion function for measuring the quality of a split and spread of estimation errors is root-mean-square error (RMSE). It quantifies the spread of these residuals (the difference between predicted and observed values/truth). While information entropy and the Gini Index are standard criterion functions for classification trees, root mean squared error (RMSE) is a popular criterion function for regression trees. RMSE is defined mathematically as the square root of the square of the average difference between the actual and predicted values:

$$RMSE = \sqrt{\sum_{i=1}^n \frac{|y_i - f(x_i)|^2}{n}} \quad (2.12)$$

Where y represents the actual observation values, $f(x_i)$ represents the estimated or predicted values, and n represents the number of data points. R-square does not tell us whether the coefficient estimates, and predictions are biased, so we must also consider the RMSE, or standard deviation of the prediction errors. For spatial autocorrelation, a widely known method used is kriging. The computational cost of kriging scales as the cube of the number of data points N , resulting in cubic time complexity for each point of interest and time complexity of $O(N^4)$ for interpolation at $O(N)$ points. One disadvantage of kriging is the high computational cost for large data sets. Local neighborhood kriging, in which only the closest observations are used for each prediction, is one approach for allowing kriging of large data. Although computationally appealing, the methods necessitate a local neighborhood for each prediction location and predicting on a fine grid is still computationally demanding. Another disadvantage is the discontinuity in prediction along the local regions' peripheries (Srinivasan et al., 2008). Several studies have proposed Random Forest regression kriging (RFRK) to account for spatial autocorrelation in Random Forest modeling (Fayad et al., 2016; Hengl et al., 2015). Regression Random Forest has been shown to be useful for spatial prediction in several studies, including (Hengl et al., 2018; Kirkwood et al., 2016; Szatmári & Pásztor, 2019; Vaysse & Lagacherie, 2017; Veronesi & Schillaci, 2019).

We use the Random Forest classifier among classifier ensembles because:

- a) it efficiently handles large databases and can run with thousands of input variables,
- b) it quantifies each input variable into a critical measure,
- c) it is robust to outliers and noise and computationally faster than other ensemble methods (Breiman, 2001; Cutler et al., 2007; Ruppert, 2004).

Chapter 3. METHODOLOGY

The primary goal of this study was to create an early screening tool for predicting potential hydrocarbon locations by utilizing gravity data by applying machine learning-assisted workflows. Previous studies, as discussed in Chapter 2, do not reflect this adequately due to the various constraints such as cost, time, and computational efficiency. The developed methodology and how it was tested are discussed in this chapter.

3.1. Research Methodology Workflow

Predicting a physical quantity of interest measured at a few sampled locations within the study region is a common problem in geosciences. Spatial prediction is used to make important decisions in many geoscience fields, such as geology, geophysics, and geochemistry. Regression Random Forest is a popular machine learning technique for spatial prediction, with competitive prediction performance in a variety of geoscience fields. Its popularity in spatial prediction stems from its ability to deal with many predictor variables efficiently, handle complex non-linear relationships and interactions, and require fewer data preprocessing. This study employs a Random Forest algorithm for the first approach, a powerful machine learning method that employs the supervised ensemble approach for both classification and regression (Breiman, 2001). As shown in Figure 3.1, this study will employ two workflows for geospatial interpolation, namely, Random Forest regression and convergent interpolation using a well-known petroleum software (Schlumberger's Petrel E & P Software Platform, v. 2020) followed by the application of Random Forest classification which was investigated for predicting different classes (oil, gas, hydrocarbon, low oil and gas, etc.). Random Forest classification uses two criteria: information entropy and the Gini Index. Entropy is a measure of disorder or uncertainty, and the Gini Index calculates the likelihood

of a specific feature being incorrectly classified when chosen at random. Random regression forest, unlike other popular machine learning methods for spatial prediction, does not consider the response variable as measured values at sampled locations (Fouedjio, 2020). To address this issue, some standard surface map interpolation techniques that account for the spatial relationship are convergent interpolation, minimum curvature, and kriging interpolation for the second approach. The convergent interpolation algorithm is used in this study to predict the values of Bouguer gravity data at locations where sampled points are lacking using a commercial software package (Schlumberger's Petrel E & P Software Platform, v. 2020).

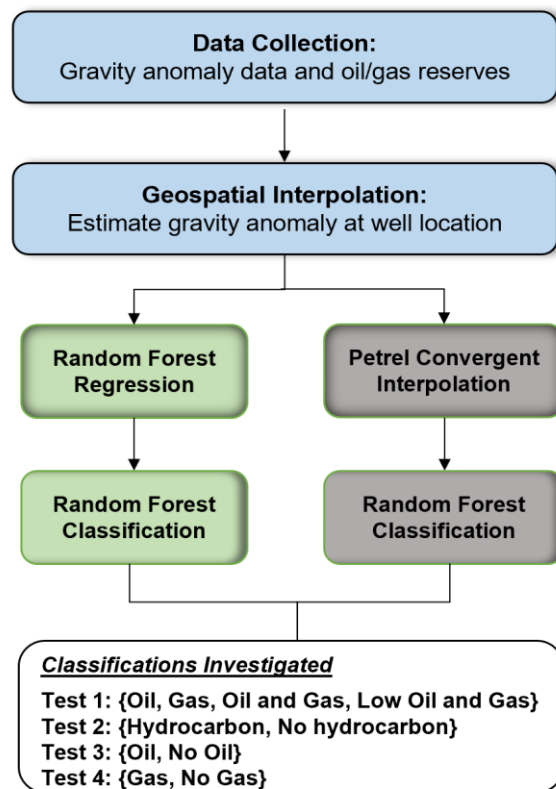


Figure 3.1. Workflow for hydrocarbon exploration classification using machine learning.

The convergent interpolation algorithm can represent geological complexity more realistically than ordinary kriging and spatial correlation, which the Random Forest algorithm may not account for (Babakhani, 2018; Fouedjio, 2020). Each iteration of the convergent interpolation algorithm (in Petrel) consists of the following three steps:

- (1) Refine - Refinement entails increasing grid resolution.
- (2) Snap - re-grid the data; and
- (3) Smooth - minimize grid curvature (Gunnarsson, 2011).

The Random Forest model is built using Python's Scikit-learn package as a framework (Pedregosa, F. and Varoquaux et al., 2011). Several model hyperparameters are tuned to improve predictive power, generalizability, and robustness. The *number of estimators = 500*, *the number of features = 3 (Latitude, Longitude, Bouguer and Isostatic gravity)*, *criterion = gini*, *min_samples_split = 2*, *min_samples_leaf = 1*, are the optimal Random Forest hyperparameters. Increasing the number of trees, for example, produces better prediction results. However, this can also slow down the model training process. The R-square (R^2) and root-mean-square error (RMSE) are used to assess model performance.

3.2. Data Collection, Preparation, and Processing

The land-based Bouguer gravity anomaly data grid for the conterminous United States (Kucks, 1999), satellite-based gravity data, and satellite-based gravity data which was enhanced through super-resolution (Zhang Yi et al., 2021) were used in this study. The training data used for the land-based gravity data prediction step was obtained from the US Geological Survey database (<https://mrdata.usgs.gov/gravity/bouguer/>). While the satellite-based gravity data were obtained

The geographical coverage includes the United States (Alabama, Alaska, Arizona, Arkansas, California, Colorado, Florida, Illinois, Indiana, Kansas, Kentucky, Louisiana, Maryland, Michigan, Mississippi, Missouri, Montana, North Dakota, Nebraska, Nevada, New Mexico, New York, Ohio, Oklahoma, Pennsylvania, South Dakota, Tennessee, Texas, Utah, Virginia, Washington, West Virginia, Wyoming). The following states do not have active or producing oil or natural gas wells, according to the Energy Information Administration (EIA): Connecticut, Delaware, District of Columbia, Georgia, Hawaii, Iowa, Idaho, Massachusetts, Maine, Minnesota, North Carolina, New Hampshire, New Jersey, Rhode Island, South Carolina, Vermont, and Wisconsin. A total of 560,000 data points were gathered. Figure 3.3 depicts a graphical representation of the regions chosen for the classification approach.

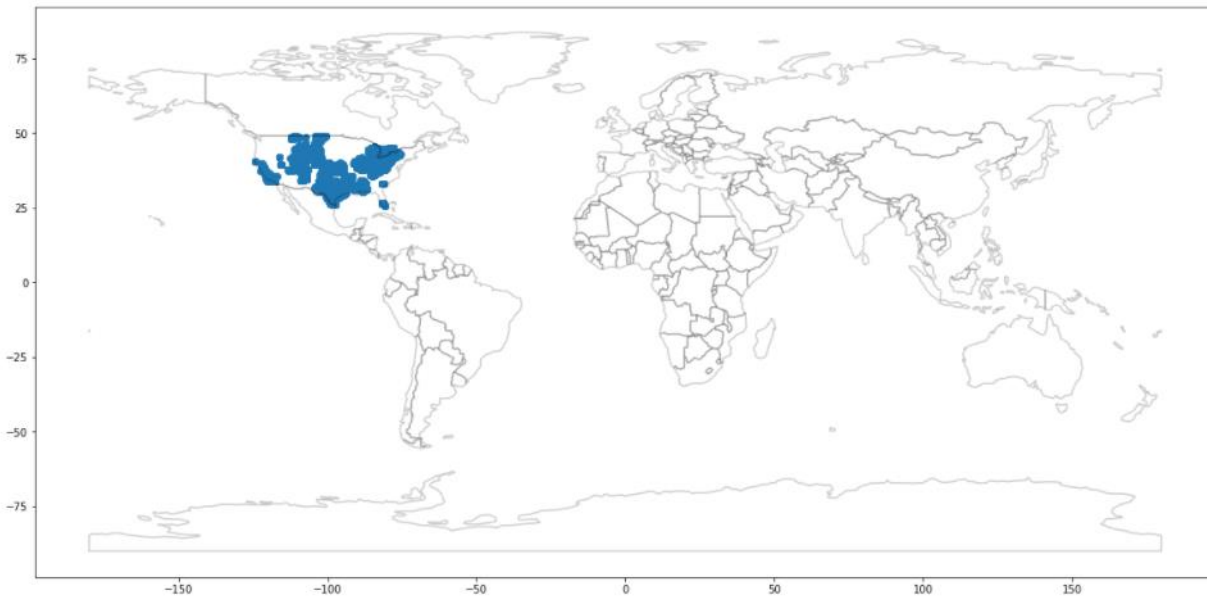


Figure 3.3. Visual representation of regions (well locations) used for the hydrocarbon classification algorithm.

Figures 3.4, 3.5, and 3.6 depict the geospatial visualization of the land-based, satellite-based and super-resolution enhanced satellite-based Bouguer and isostatic gravity anomaly map. Longitude and latitude were extracted using the ArcGIS software platform. In ArcGIS, the geographic coordinates were converted to a standard reference projection, WGS 1984 (EPSG 4326) (Keller, 1995). The Random Forest model uses the oil/gas field's latitude and longitude coordinates, Bouguer gravity values as the input features and hydrocarbon classifications as the output features (oil, gas, both gas and oil, and low-volume hydrocarbons).

In addition to the case mentioned above, we evaluated the implementation of the oil/gas field's Bouguer gravity, isostatic, and free-air gravity values as the input features without including their latitude and longitude coordinates and different combinations of hydrocarbon classifications as the output features, such as, hydrocarbon versus no hydrocarbons, oil versus no oil, and gas versus no gas, as well as all four classes of oil, gas, oil and gas, and low hydrocarbons. The implementation of an unsupervised machine learning model, Self-Organizing Map (SOM), was also evaluated to evaluate its applicability in the classification of hydrocarbon regions.

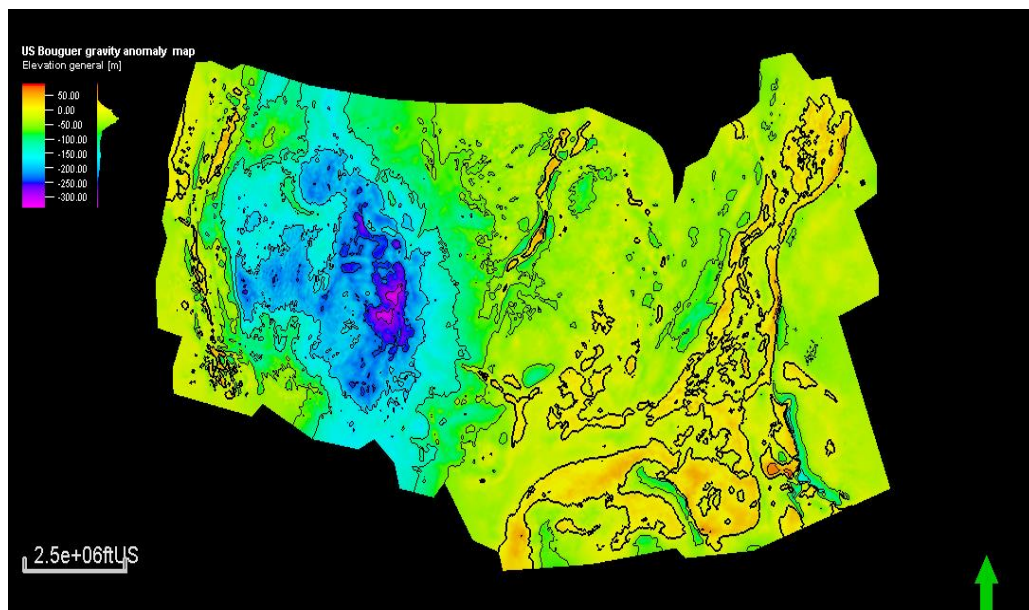


Figure 3.4. US land based Bouguer gravity anomaly map (in mgals).

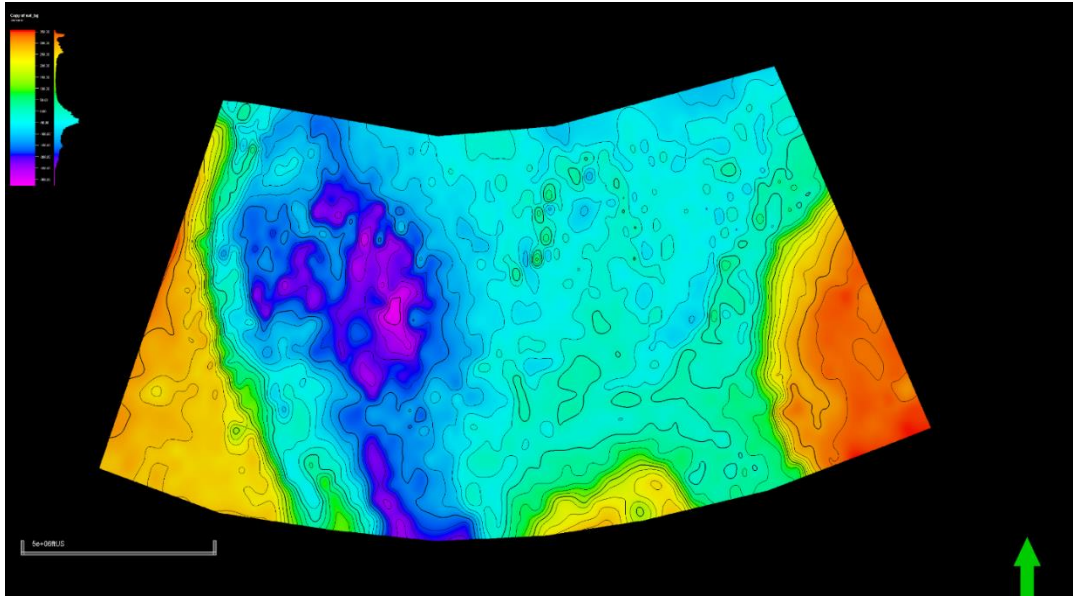


Figure 3.5. US satellite based Bouguer gravity anomaly map (in mgals)

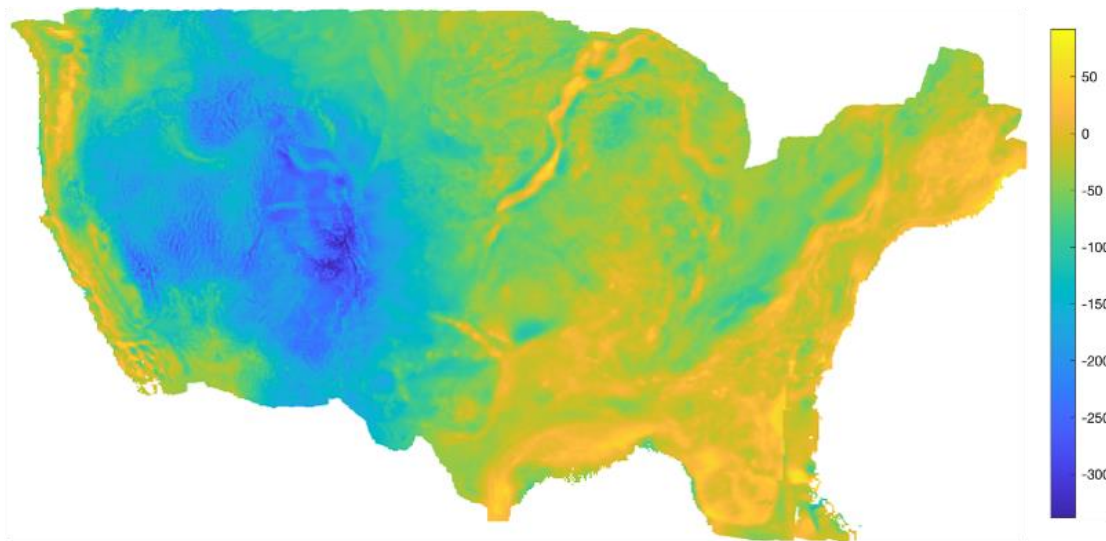


Figure 3.6. Enhanced US satellite based Bouguer gravity anomaly map (in mgals) using super-resolution algorithm (Zhang Yi et al., 2021).

The low-volume hydrocarbons class is defined by proven hydrocarbon reserves and includes reservoirs with reserves volumes estimated to be less than 10 MBOE (thousands of barrels of oil equivalent) which typically indicates an uneconomic hydrocarbon play. Using Python's Scikit-learn Label Encoder module, the four classes of gas, gas and oil, low-volume hydrocarbons, and oil were labeled as 0, 1, 2, and 3, respectively. The dataset is divided into three parts for hydrocarbon classification: training, validation, and testing. The Bouguer and Isostatic gravity prediction input features are randomly divided into 70% and 30% splits for training and testing, respectively for geospatial interpolation. The hydrocarbon classification training datasets are randomly divided into 60%, 20%, and 20% splits for training and validation and testing, respectively. For the other different output target classes evaluated, namely, hydrocarbon versus no hydrocarbons, oil versus no oil, and gas versus no gas. A train/test split ratio of 80/20 was used for the Random Forest classification. In addition, a small test set from a region not included in the training and test dataset was processed through the model to evaluate the generalizability of the model to predict hydrocarbon deposits in other geographical locations.

3.3. Classification Accuracy Assessment

The Random Forest calibration model and output results were evaluated using F1 accuracy, the harmonic mean of precision, and sensitivity (recall) accuracy statistics. They are used to calculate the Random Forest calibration's out-of-bag error. Precision is defined as the proportion of correctly predicted positive classes to the total number of positive observations (incorporating true positives and false positives). Simultaneously, recall is defined as the ratio of correctly predicted positive observations to the sum of true positives and false negatives. This, on the other hand, can be interpreted as a measure of the truly assigned field to a specific class (recall). The F1 score is a

robust accuracy measure for model performance because it balances the influence of recall and precision using the harmonic mean of both, as shown by the formulae below:

$$F1\ Accuracy = 2 * \frac{Precision * Recall}{Recall + Precision} \quad (3.1)$$

$$Precision = \frac{TP}{TP + FP} \quad (3.2)$$

$$Recall = \frac{TP}{TP + FN} \quad (3.3)$$

Where $TP = True\ positives$, $FP = False\ positives$, and $FN = False\ negatives$.

Chapter 4. RESULTS

4.1. Land-based Gravity Anomaly Prediction

The first goal entails the prediction of Bouguer and isostatic gravity values at different well locations. Two different methods were evaluated to achieve this: using Random Forest regression machine learning model approach and using a geospatial interpolation algorithm implemented through a commercial software (Petrel E&P v 2020).

For Bouguer gravity interpolation, the latitude and longitude coordinates of the hydrocarbon wells are used as input features in training the Random Forest regression model, while the collected Bouguer gravity is used as the target feature. Table 4.1 contains information about the ranges for the input parameters used. The number of data points for each defined hydrocarbon class is shown in Table 4.2. The RMSE and R-square values, which are summarized in Table 4.3, are used to compare the resulting performance of the trained model and prediction. On the training dataset, the trained model had an R-square accuracy of 99.99% with an RMSE value of 0.77 mgal, while on the test dataset, it had an R-square accuracy of 99.91% with an RMSE value of 2.02 mgal. When predicting for the test dataset, the spread of residual errors increased, as evidenced by the RMSE value of Bouguer gravity test prediction model. The Random Forest regression model's two input features for isostatic gravity prediction are the hydrocarbon field's latitude and longitude coordinates. The isostatic trained model had an R-square accuracy of 99.8% with an RMSE value of 0.7650 mgal on the training dataset and an R-square accuracy of 98.9% with an RMSE value of 2.0112 mgal on the test dataset, as shown in Table 4.4. It demonstrates that the RMSE (spread of residual errors) of the isostatic gravity test prediction model increases when predicting for the test datasets.

Table 4.1. Range of input features

Number of Bouguer gravity data points	722,941
Isostatic gravity data range	-204.199 to 104.16 mgal
Bouguer gravity data range	-338.25 to 92.0478 mgal
Oil/gas reserves Latitude range	23.562 ⁰ to 49.415 ⁰
Oil/gas reserves Longitude range	-127.641 ⁰ to -64.423 ⁰

Table 4.2. Number of data points in the different classes

Hydrocarbon class	Number of data points
Low-volume hydrocarbons (<10MBOE)	140,000
Gas	140,000
Oil	140,000
Gas and Oil	140,000

Table 4.3. Random Forest regression results for Bouguer land-based gravity prediction

	X (no. of datapoints, no. of features)	Y (no. of datapoints)	R ²	RMSE (mgal)
Train dataset	(506058, 2)	506058	0.9998	0.7717
Test dataset	(216883, 2)	216883	0.9991	2.0189

Table 4.4. Random Forest regression results for isostatic gravity prediction

	X (no. of datapoints, no. of features)	Y (no. of datapoints)	R^2	RMSE (mgal)
Train dataset	(506058,2)	506058	0.9984	0.7677
Test dataset	(216883, 2)	216883	0.9894	2.0112

The second approach for gravity anomaly interpolation was using geospatial kriging using convergent interpolation algorithm implemented using a commercial software (Petrel E&P v. 2000). Figure 4.1 depicts how the convergent interpolation algorithm can be used to predict the Bouguer gravity data values at different locations. A similar approach was used to predict the isostatic gravity anomaly values at the different well locations.

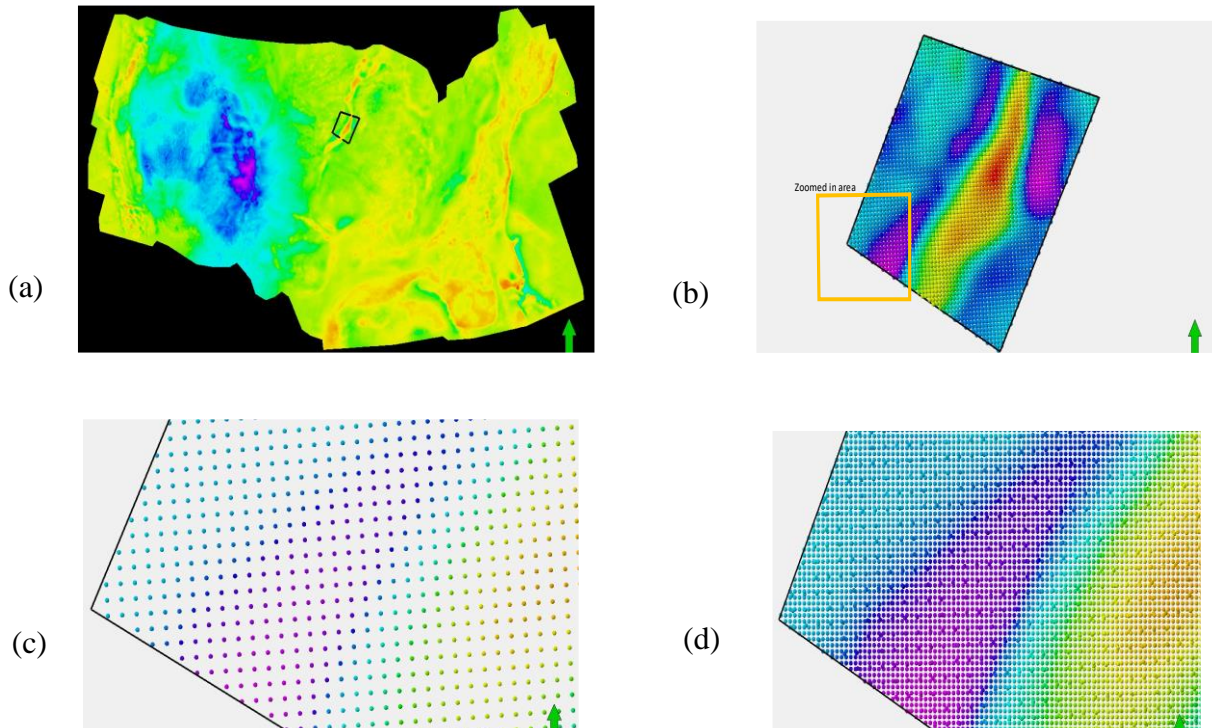


Figure 4.1. (a) Bouguer gravity anomaly map for the United States (b) Section chosen for interpolation. (c) A zoomed-in section of the Bouguer gravity data points (d) Interpolated Bouguer gravity data points filled in with geospatial trend.

After grid refinement, we can use Petrel's convergent interpolation to interpolate the Bouguer data values within a polygon field, as shown in figure 4.2.

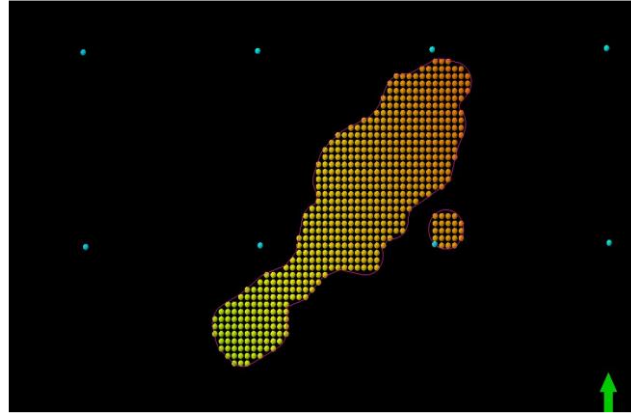


Figure 4.2. Convergent interpolated Bouguer gravity points within polygon field.

4.1.1. Land-based Hydrocarbons Classification Results

Several different combinations of input features and output classes were tested and compared for hydrocarbon classification, using both supervised and unsupervised machine learning, as summarized below.

Input features evaluated:

1. Bouguer gravity (interpolated using Random Forest)
2. Bouguer gravity (interpolated using Petrel convergent interpolation)
3. Isostatic gravity (interpolated using Random Forest)
4. Isostatic gravity (interpolated using Petrel convergent interpolation)
5. Latitude and Longitude coordinates

Output classes evaluated:

1. Oil, Gas, Oil and Gas, Low-volume Hydrocarbon
2. Hydrocarbon, No Hydrocarbon
3. Oil, No Oil
4. Gas, No Gas

In the first approach, the input features are the Bouguer and isostatic anomaly gravity values at the hydrocarbon fields and well locations (both interpolated using the Random Forest regression), and the hydrocarbon fields' latitude and longitude coordinates. The target output classes are gas, gas and oil, low-volume hydrocarbons, and oil. A train/validation/test split ratio of 60/20/20 is used for the classification model. Tables 4.5, 4.6 and 4.7 summarize the comparison of the classification model's resulting performance using its F1-score, precision, and recall values. The results show that the trained model had an average F1-score accuracy of 99.99% on the training dataset and roughly 89.82% on the validation and roughly 89.75% on the test dataset. According to the test results confusion matrix in Table 4.8. 23,948 Gas labels were correctly classified, as well as 23,797 Gas and Oil labels, 27428 Low volume hydrocarbon labels, and 25,347 Oil labels were correctly classified.

Table 4.5. Random Forest hydrocarbon classification train dataset report

	Precision	Recall	F1-score	support
Gas	1.00	1.00	1.00	83986
Gas and Oil	1.00	1.00	1.00	84010
Low-volume Hydrocarbons	1.00	1.00	1.00	84000
Oil	1.00	1.00	1.00	84004
Accuracy			0.9999	336000

Table 4.6. Random Forest hydrocarbon classification validation dataset report

	Precision	Recall	F1-score	support
Gas	0.86	0.88	0.87	27346
Gas and Oil	0.85	0.86	0.85	27868
Low-volume Hydrocarbons	0.98	0.96	0.97	28569
Oil	0.91	0.90	0.90	28217
Accuracy			0.8982	112000

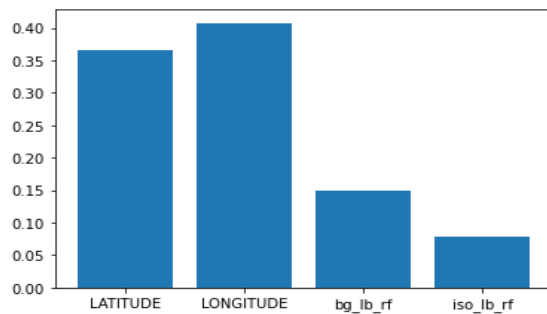
Table 4.7. Random Forest hydrocarbon classification test dataset report

	Precision	Recall	F1-score	support
Gas	0.86	0.87	0.86	27502
Gas and Oil	0.85	0.86	0.85	27767
Low-volume Hydrocarbons	0.98	0.96	0.97	28566
Oil	0.91	0.90	0.90	28165
Accuracy			0.8975	112000

Table 4.8. Hydrocarbon classification confusion matrix for test dataset

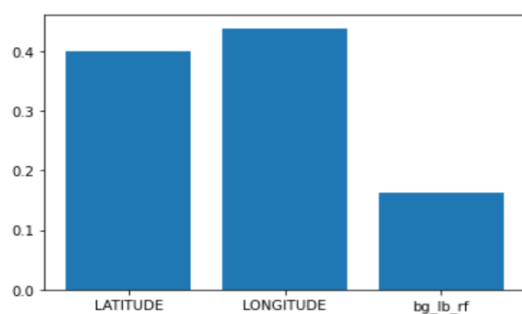
Class	Gas	Gas and Oil	Low-volume Hydrocarbons	Oil
Gas	23948	2162	157	1235
Gas and Oil	2282	23797	365	1323
Low-volume Hydrocarbons	455	588	27428	95
Oil	1315	1453	50	25347

In this case, the isostatic gravity had minor feature importance for the classification model, as shown in Figure 4.3. The input feature importance with just Bouguer gravity, latitude, and longitude is shown in Figure 4.4.



Input features	Feature_Importance_Score
Bouguer gravity	0.14841
Isostatic gravity	0.07861
Latitude	0.36538
Longitude	0.40760

Figure 4.3. Isostatic gravity Random Forest classification model feature importance



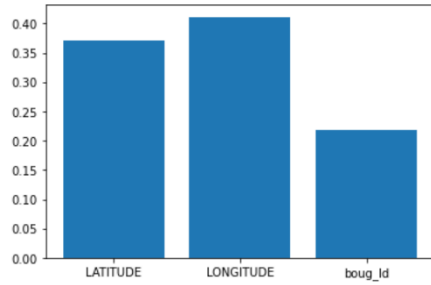
Input features	Feature_Importance_Score
Bouguer gravity	0.16263
Latitude	0.39922
Longitude	0.43815

Figure 4.4. Random Forest classification model features importance

In the next approach, the input features included the Bouguer gravity values at the hydrocarbon field and well locations predicted using Petrel's convergent interpolation algorithm for geospatial kriging, along with the latitude and longitude values, while the output classes were gas, gas and oil, low-volume hydrocarbons, and oil. This time, the isostatic gravity was not included as an input feature. Table 4.9 shows the hydrocarbon classification results using Petrel's interpolated Bouguer gravity data to account for its geospatial trend and the feature importance input parameters is shown in Figure 4.5.

Table 4.9. Petrel hydrocarbon classification testing dataset report

	Precision	Recall	F1-score	support
Gas	0.86	0.87	0.86	27419
Gas and Oil	0.85	0.85	0.85	27818
Low-volume Hydrocarbons	0.98	0.97	0.97	28408
Oil	0.90	0.89	0.89	28355
Accuracy			0.8965	112000



Input features	Feature Importance Score
Bouguer gravity	0.21873
Latitude	0.37028
Longitude	0.41099

Figure 4.5. Petrel hydrocarbon classification model features importance

The third approach involved using both the Bouguer and isostatic anomaly gravity values at the hydrocarbon field and well location, interpolated either using Random Forest regression or Petrel convergent interpolation, as the input features for the classifications, but this time latitude and longitude coordinates were not included as input features. Different output target classes were evaluated, namely, hydrocarbon versus no hydrocarbons, oil versus no oil, and gas versus no gas. A train/test split ratio of 80/20 was used for the Random Forest classification. In addition, a small test set from a region not included in the training and test dataset was processed through the model to evaluate the generalizability of the model to predict hydrocarbon deposits in other geographical locations. Tables 4.10 to 4.15, summarizes the results of the comparison of the classification model's resulting performance using its F1-score accuracy values. For completion, the results from the previous two approaches (that included latitude and longitude as input feature) are also included for comparison. The results show that the trained model for different input features and output classes of hydrocarbon vs no hydrocarbon had an average F1-score accuracy of 100% on the training dataset and roughly an average of 98% on the test dataset and roughly an average of 71% on the blind test dataset. For oil vs no oil classification, the results show that the trained model had an average F1-score accuracy of 92.25% on the training dataset and roughly an average of 77.5% on the test dataset and roughly an average of 55.25% on the blind test dataset. Lastly, for

gas vs no gas classification, the results show that the trained model had an average F1-score accuracy of 91.75% on the training dataset and roughly an average of 72.5% on the test dataset and roughly an average of 52.75% on the blind test dataset. Among the different reserve class combinations predicted, the hydrocarbon versus no hydrocarbon class prediction gave the best overall accuracy in both the testing and blind testing data (in a different geographical location). The lower accuracy results for the blind testing set indicates that more geological parameters (beyond the gravity anomaly values) are likely needed to predict the presence of hydrocarbons with higher accuracy. Additional features such as seismic data, well log information, or other geological data could be included in future work.

The implementation of an unsupervised machine learning model, Self-Organizing Map (SOM), was also evaluated to test its applicability in the classification of hydrocarbon regions for different combinations of the input features and output classes. The results summarized in Tables 4.10 to 4.15 show that the use of the SOM model generates low accuracy compared to the Random Forest model. This indicates that the use of unsupervised learning is not sufficient to map the gravity estimates to hydrocarbon classes and supervised machine learning approach provides better prediction accuracy.

Table 4.10. Land-based hydrocarbons vs no hydrocarbons classification training results

Land based - Hydrocarbons vs No Hydrocarbons (HC vs nHC)													
		Train set F1-score accuracy						Blind test set F1-score accuracy					
Model		Random Forest			Petrel			Random Forest			Petrel		
Input features		Overall	HC	nHC	Overall	HC	nHC	Overall	HC	nHC	Overall	HC	nHC
Train/test split ratio: 80/20	Bouguer gravity	100%	100%	100%	76%	75%	77%	68%	73%	61%	72%	75%	66%
	Bouguer & Isostatic gravity	100%	100%	100%	100%	100%	100%	71%	77%	62%	71%	77%	62%
	Latitude, Longitude & Bouguer gravity	100%	100%	100%	100%	100%	100%	70%	77%	57%	72%	78%	61%
	Latitude, Longitude, Bouguer and Isostatic gravity	100%	100%	100%	100%	100%	100%	71%	77%	59%	72%	78%	57%
Self-Organizing Map	Bouguer gravity	43.95%	55%	26%	43.97%	55%	26%	53.50%	13%	68%	53.63%	14%	68%
	Bouguer & Isostatic gravity	56.01%	42%	65%	44.06%	55%	26%	45.99%	63%	0%	53.97%	15%	68%
	Latitude, Longitude & Bouguer gravity	43.09%	54%	26%	56.59%	43%	65%	53.39%	13%	68%	47%	64%	0%
	Latitude, Longitude, Bouguer and Isostatic gravity	56.63%	43%	65%	43.59%	54%	26%	46.21%	63%	0%	54%	14%	68%

Table 4.11. Land-based hydrocarbons vs no hydrocarbons classification testing results

Land based - Hydrocarbons vs No Hydrocarbons (HC vs nHC)													
		Test set F1-score accuracy						Blind test set F1-score accuracy					
Model		Random Forest			Petrel			Random Forest			Petrel		
Input features		Overall	HC	nHC	Overall	HC	nHC	Overall	HC	nHC	Overall	HC	nHC
Train/test split ratio: 80/20	Bouguer gravity	79%	78%	79%	73%	72%	74%	68%	73%	61%	72%	75%	66%
	Bouguer & Isostatic gravity	91%	91%	91%	87%	87%	88%	71%	77%	62%	71%	77%	62%
	Latitude, Longitude & Bouguer gravity	98%	98%	98%	98%	99%	98%	70%	77%	57%	72%	78%	61%
	Latitude, Longitude, Bouguer and Isostatic gravity	98%	98%	99%	98%	98%	98%	71%	77%	59%	72%	78%	57%
Self-Organizing Map	Bouguer gravity	43.95%	55%	26%	43.97%	55%	26%	53.50%	13%	68%	53.63%	14%	68%
	Bouguer & Isostatic gravity	56.01%	42%	65%	44.06%	55%	26%	45.99%	63%	0%	53.97%	15%	68%
	Latitude, Longitude & Bouguer gravity	43.09%	54%	26%	56.59%	43%	65%	53.39%	13%	68%	47%	64%	0%
	Latitude, Longitude, Bouguer and Isostatic gravity	56.63%	43%	65%	43.59%	54%	26%	46.21%	63%	0%	54%	14%	68%

Table 4.12. Land-based oil vs no oil classification training results

Land based - Oil vs No Oil (O vs nO)													
		Train set F1-score accuracy						Blind test set F1-score accuracy					
Model		Random Forest			Petrel			Random Forest			Petrel		
Input features		Overall	O	nO	Overall	O	nO	Overall	O	nO	Overall	O	nO
Train/test split ratio: 80/20	Bouguer gravity	99%	99%	99%	71%	70%	71%	54%	56%	52%	54%	57%	51%
	Bouguer & Isostatic gravity	99%	99%	99%	100%	100%	100%	57%	61%	51%	56%	59%	52%
Self-Organizing Map	Bouguer gravity	61.53%	33%	73%	62.37%	34%	74%	26.02%	39%	6%	26.03%	39%	7%
	Bouguer & Isostatic gravity	38.54%	34%	43%	61.96%	33%	73%	74.23%	13%	85%	25.89%	38%	8%
	Latitude, Longitude & Bouguer gravity	59.88%	33%	71%	39.39%	33%	44%	25%	39%	6%	74.03%	12%	85%
	Latitude, Longitude, Bouguer and Isostatic gravity	59.95%	33%	72%	39.44%	34%	44%	25.95%	39%	7%	74.08%	13%	85%

Table 4.13. Land-based oil vs no oil classification testing results

Land based - Oil vs No Oil (O vs nO)													
		Test set F1-score accuracy						Blind test set F1-score accuracy					
Model		Random Forest			Petrel			Random Forest			Petrel		
Input features		Overall	O	nO	Overall	O	nO	Overall	O	nO	Overall	O	nO
Train/test split ratio: 80/20	Bouguer gravity	73%	73%	73%	64%	64%	65%	54%	56%	52%	54%	57%	51%
	Bouguer & Isostatic gravity	88%	88%	88%	85%	85%	85%	57%	61%	51%	56%	59%	52%
Self-Organizing Map	Bouguer gravity	61.53%	33%	73%	62.37%	34%	74%	26.02%	39%	6%	26.03%	39%	7%
	Bouguer & Isostatic gravity	38.54%	34%	43%	61.96%	33%	73%	74.23%	13%	85%	25.89%	38%	8%
	Latitude, Longitude & Bouguer gravity	59.88%	33%	71%	39.39%	33%	44%	25%	39%	6%	74.03%	12%	85%
	Latitude, Longitude, Bouguer and Isostatic gravity	59.95%	33%	72%	39.44%	34%	44%	25.95%	39%	7%	74.08%	13%	85%

Table 4.14. Land-based gas vs no gas classification training results

Land based - Gas vs No Gas (G vs nG)													
		Train set F1-score accuracy						Blind test set F1-score accuracy					
Model		Random Forest			Petrel			Random Forest			Petrel		
Input features		Overall	G	nG	Overall	G	nG	Overall	G	nG	Overall	G	nG
Train/test split ratio: 80/20	Bouguer gravity	99%	99%	99%	69%	68%	69%	52%	55%	48%	52%	55%	50%
	Bouguer & Isostatic gravity	99%	99%	99%	100%	100%	100%	53%	47%	58%	53%	46%	59%
Self-Organizing Map	Bouguer gravity	42.13%	37%	46%	41.06%	37%	45%	74.32%	11%	85%	73.83%	12%	85%
	Bouguer & Isostatic gravity	57.97%	27%	7%	41.18%	37%	45%	26.24%	37%	7%	73.31%	12%	84%
	Latitude, Longitude & Bouguer gravity	43.66%	38%	49%	57.26%	27%	70%	74.32%	11%	85%	25.99%	39%	8%
	Latitude, Longitude, Bouguer and Isostatic gravity	43.59%	38%	48%	57.34%	27%	70%	74%	11%	85%	26%	39%	7%

Table 4.15. Land-based gas vs no gas classification training results

Land based - Gas vs No Gas (G vs nG)													
		Train set F1-score accuracy						Blind test set F1-score accuracy					
Model		Random Forest			Petrel			Random Forest			Petrel		
Input features		Overall	G	nG	Overall	G	nG	Overall	G	nG	Overall	G	nG
Train/test split ratio: 80/20	Bouguer gravity	67%	67%	67%	62%	61%	63%	52%	55%	48%	52%	55%	50%
	Bouguer & Isostatic gravity	82%	82%	82%	79%	79%	79%	53%	47%	58%	53%	46%	59%
Self-Organizing Map	Bouguer gravity	42.13%	37%	46%	41.06%	37%	45%	74.32%	11%	85%	73.83%	12%	85%
	Bouguer & Isostatic gravity	57.97%	27%	7%	41.18%	37%	45%	26.24%	37%	7%	73.31%	12%	84%
	Latitude, Longitude & Bouguer gravity	43.66%	38%	49%	57.26%	27%	70%	74.32%	11%	85%	25.99%	39%	8%
	Latitude, Longitude, Bouguer and Isostatic gravity	43.59%	38%	48%	57.34%	27%	70%	74%	11%	85%	26%	39%	7%

4.2. Satellite-based Gravity Anomaly Prediction Results

In this case, the input gravity anomalies were derived from satellite-based earth gravity model datasets which were obtained from the ICGEM website (<http://icgem.gfz-potsdam.de/calgrid>). Similar to the land-based gravity modelling case, the gravity anomalies were interpolated using two different approaches, using Random Forest regression and Petrel convergent interpolation. The gravity anomalies predicted at the hydrocarbon field and well locations were subsequently used for predicting different hydrocarbon classes using Random Forest classification.

The latitude and longitude coordinates at the hydrocarbon field and well locations are used to train a Random Forest regression model, with satellite derived Bouguer gravity values serving as the target outputs. Table 4.16 contains information about the input parameter data. Similarly, the RMSE and R-square values summarized in Table 4.17 are used to compare the resulting performance of the trained model and prediction. On the training dataset, the trained model had an R-square accuracy of 99.51% with an RMSE value of 10.42, while on the test dataset, it had an R-square accuracy of 96.96% with an RMSE value of 26.08.

Table 4.16. Range of input features

Number of Bouguer gravity data points	1500
Bouguer gravity data range	-320.19 to 355.393 mgal
Hydrocarbons Latitude range	25.039 ⁰ to 49.039 ⁰
Hydrocarbons Longitude range	-126.169 ⁰ to -67.17 ⁰

Table 4.17. Random Forest regression results for satellite based Bouguer gravity prediction

	X (no. of datapoints, no. of features)	Y (no. of datapoints)	R^2	RMSE (mgal)
Train dataset	(1050, 2)	1050	0.9951	10.42
Test dataset	(450, 2)	450	0.9696	26.08

The interpolation approach using Petrel convergent algorithm was similar to the one used for land-based gravity, as described in section 4.1 (and therefore not repeated here).

4.2.1. Satellite-based Hydrocarbons Classification Results

Similar to the hydrocarbon classification using land-based gravity (described in Sec. 4.1.1.), in this case also several different combinations of input features and output classes were tested and compared for hydrocarbon classification, using both supervised and unsupervised machine learning.

In the first approach, satellite-based Bouguer gravity (interpolated using Random Forest regression), as well as the latitude and longitude at the well and field locations, were used as the input features, while the output classes were oil, gas, oil and gas, and low-volume hydrocarbons. Tables 4.18, 4.19, and 4.20 summarize a comparison of the classification model's resulting performance using its F1-score, precision, and recall values after predicting the Bouguer gravity values at the location of the hydrocarbon fields. According to the results, the trained model had an F1-score accuracy of roughly 99.99% on the training dataset and roughly 89.52% on the validation dataset, and roughly 89.62% on the test dataset. According to the test results confusion matrix in

Table 4.21, 23,968 gas labels were correctly classified, as well as 23,786 gas and oil labels, 27427 low-volume hydrocarbon labels, and 25,427 Oil labels were correctly classified.

Table 4.18. Random Forest hydrocarbons classification training dataset report

	Precision	Recall	F1-score	support
Gas	1.00	1.00	1.00	83986
Gas and Oil	1.00	1.00	1.00	84010
Low-volume Hydrocarbons	1.00	1.00	1.00	84000
Oil	1.00	1.00	1.00	84004
Accuracy			0.9999	336000

Table 4.19. Random Forest hydrocarbon classification validation dataset report

	Precision	Recall	F1-score	support
Gas	0.86	0.88	0.87	27315
Gas and Oil	0.85	0.86	0.85	27830
Low-volume Hydrocarbons	0.98	0.96	0.97	28574
Oil	0.91	0.90	0.90	28281
Accuracy			0.8952	112000

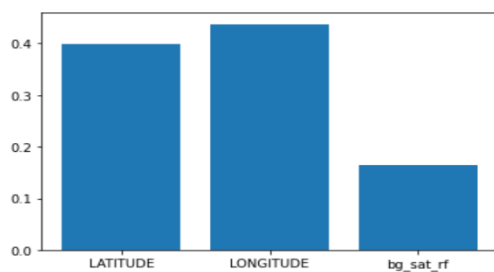
Table 4.20. Random Forest hydrocarbon classification test dataset report

	Precision	Recall	F1-score	support
Gas	0.86	0.87	0.86	27489
Gas and Oil	0.85	0.86	0.85	27702
Low-volume Hydrocarbons	0.98	0.96	0.97	28549
Oil	0.91	0.90	0.90	28260
Accuracy			0.8962	112000

Table 4.21. Hydrocarbon classification confusion matrix for test dataset

Class	Gas	Gas and Oil	Low-volume Hydrocarbons	Oil
Gas	23968	2156	159	1206
Gas and Oil	2262	23786	367	1287
Low-volume Hydrocarbons	450	592	27427	80
Oil	1320	1466	47	25427

Figure 4.6 depicts the model input feature importance for the latitude, longitude and Bouguer gravity values.



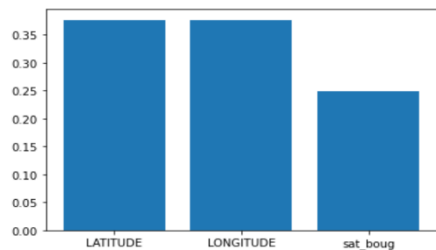
Input features	Feature Importance Score
Bouguer gravity	0.16414
Latitude	0.39856
Longitude	0.43730

Figure 4.6. Random Forest hydrocarbon classification model features importance

In the next approach, the input features included the Bouguer gravity (interpolated using Petrel convergent interpolation algorithm) and the latitude and longitude of the well and field locations. The output classes were oil, gas, oil and gas, and low-volume hydrocarbons. Table 4.22 shows the hydrocarbon classification results using Petrel’s interpolated Bouguer gravity data to account for its geospatial trend and the input feature importance is shown in Figure 4.7.

Table 4.22. Petrel hydrocarbon classification testing dataset report

	Precision	Recall	F1-score	support
Gas	0.85	0.87	0.86	27390
Gas and Oil	0.85	0.85	0.85	27749
Low-volume Hydrocarbons	0.98	0.97	0.98	284648
Oil	0.90	0.89	0.90	28393
Accuracy			0.8961	112000



Input features	Feature Importance Score
Bouguer gravity	0.24802
Latitude	0.37574
Longitude	0.37624

Figure 4.7. Petrel hydrocarbon classification model features importance

The next approach involved using both the Bouguer gravity and free-air gravity values (interpolated using Petrel convergent interpolation algorithm) as the Random Forest classifier model's input features, and the latitude and longitude coordinates were not included as input features. The free-air gravity was used in place of isostatic gravity as the isostatic gravity dataset was not readily available from satellite data. Different output classes were evaluated, namely, hydrocarbon versus no hydrocarbons, oil versus no oil, and gas versus no gas. The classification input data used a train/test split ratio of 80/20. Tables 4.23, 4.24, and 4.25 summarize the comparison of the classification model's resulting performance using its F1-score accuracy values for different input features. The hydrocarbon vs no hydrocarbon had an average F1-score accuracy of 90% on the training dataset and roughly an average of 85% on the test dataset and roughly an average of 68% on the blind test dataset. For oil vs no oil classification, the results show that the trained model had an average F1-score accuracy of 87% on the training dataset and roughly an average of 78.5% on the test dataset and roughly an average of 51.5% on the blind test dataset. Lastly, for gas vs no gas classification, the results show that the trained model had an average F1-score accuracy of 86% on the training dataset and roughly an average of 74.5% on the test dataset and roughly an average of 49% on the blind test dataset. Similar to the land-based gravity case, the prediction for hydrocarbon versus no hydrocarbon was the best among the class combinations tested. The results for the blind testing at a different geographical location are not as robust, indicating the need for including additional input features for hydrocarbon prediction at a new location.

Table 4.23. Satellite-based hydrocarbons vs no hydrocarbons classification results

Satellite - Hydrocarbons vs No Hydrocarbons (HC vs nHC)										
		Train set F1-score accuracy			Test set F1-score accuracy			Blind test set F1-score accuracy		
Model		Petrel			Petrel			Petrel		
Input features		Overall	HC	nHC	Overall	HC	nHC	Overall	HC	nHC
Train/test split ratio: 80/20	Bouguer gravity	80%	79%	81%	77%	76%	78%	70%	75%	73%
	Bouguer & free-air gravity	100%	100%	100%	93%	93%	93%	66%	74%	54%

Table 4.24. Satellite-based oil vs no oil classification results

Satellite - Oil vs No Oil (O vs nO)										
		Train set F1-score accuracy			Test set F1-score accuracy			Blind test set F1-score accuracy		
Model		Petrel			Petrel			Petrel		
Input features		Overall	O	nO	Overall	O	nO	Overall	O	nO
Train/test split ratio: 80/20	Bouguer gravity	74%	75%	73%	69%	70%	68%	52%	55%	49%
	Bouguer & free-air gravity	100%	100%	100%	88%	89%	88%	51%	53%	48%

Table 4.25. Satellite-based gas vs no gas classification results

Satellite - Gas vs No Gas (G vs nG)										
		Train set F1-score accuracy			Test set F1-score accuracy			Blind test set F1-score accuracy		
Model		Petrel			Petrel			Petrel		
Input features		Overall	G	nG	Overall	G	nG	Overall	G	nG
Train/test split ratio: 80/20	Bouguer gravity	72%	72%	71%	66%	67%	65%	48%	48%	47%
	Bouguer & free-air gravity	100%	100%	100%	83%	83%	84%	50%	48%	52%

4.3. Enhanced Satellite-based Bouguer Gravity Prediction Results

In this case, the input gravity anomalies were derived from satellite-based earth gravity model data, which was enhanced through deep learning based super resolution obtained from reference Zhang Yi et al. (2021). Similar to the land-based and satellite-based gravity modeling cases, the super-resolution enhanced-satellite gravity anomalies were interpolated using two different approaches, using Random Forest regression and Petrel convergent interpolation. The gravity anomalies predicted at the hydrocarbon field and wellbore locations were subsequently used for predicting different hydrocarbon classes using Random Forest classification.

The latitude and longitude coordinates of the hydrocarbon field and well locations are used as input features in training the Random Forest regression model, while the collected Bouguer gravity is used as the target feature. Table 4.26 contains information about the input parameter data. The RMSE and R-square values, which are summarized in Tables 4.27 and 4.28, are used to compare the resulting performance of the trained model and prediction. On the training dataset, the trained model had an R-square accuracy of 99.99% with an RMSE value of 0.456 mgal, while on the test

dataset, it had an R-square accuracy of 99.95% with an RMSE value of 1.204 mgal. According to the RMSE value of Bouguer gravity test prediction model, the spread of residual errors increased when predicting for the test datasets. The free-air gravity anomaly trained model had an R-square accuracy of 99.9% with an RMSE value of 0.456 mgal on the training dataset and an R-square accuracy of 99.9% with an RMSE value of 1.200 mgal on the test dataset, as shown in Table 4.28. It demonstrates that the RMSE (spread of residual errors) of the free-air gravity test prediction model increases when predicting for the test datasets.

Table 4.26. Range of input features

Number of Bouguer gravity data points	2,854,368
Bouguer gravity data range	-338.12 to 92.49 mgal
Oil/gas reserves Latitude range	31.389 ⁰ to 49.42 ⁰
Oil/gas reserves Longitude range	-127.639 ⁰ to -64.495 ⁰

Table 4.27. Random Forest regression results for Bouguer gravity prediction

	X (no. of datapoints, no. of features)	Y (no. of datapoints)	R ²	RMSE (mgal)
Train dataset	(1998057, 2)	1998057	0.9999	0.456
Test dataset	(856311, 2)	856311	0.9995	1.204

Table 4.28. Random Forest regression results for free-air gravity prediction

	X (no. of datapoints, no. of features)	Y (no. of datapoints)	R^2	RMSE (mgal)
Train dataset	(1998057, 2)	1998057	0.9994	0.458
Test dataset	(856311, 2)	856311	0.9965	1.200

Both the Bouguer and free-air gravity anomalies were also interpolated using Petrel convergent algorithm for geospatial kriging in a similar manner as the land-based gravity. This method was described in section 4.1 (and therefore not repeated here).

4.3.1. Enhanced Satellite-based Hydrocarbons Classification Results

Similar to the hydrocarbon classification using land-based and satellite-based gravity described in Sections 4.1 and 4.2, in this case also several different combinations of input features and output classes were tested and compared for hydrocarbon classification, using both supervised and unsupervised machine learning.

In the first approach, satellite-based Bouguer gravity (interpolated using Random Forest regression), as well as the latitude and longitude information at the well and hydrocarbon field locations, were used as the input features, while the output classes were oil, gas, oil and gas, and low-volume hydrocarbons. Tables 4.29, 4.30 and 4.31 summarize a comparison of the classification model's resulting performance using its F1-score, precision, and recall values. According to the results, the trained model had an F1-score accuracy of 99.99% on the training dataset and roughly 89.82% on the validation dataset and roughly 89.80% on the test dataset. According to the test results confusion matrix in Table 4.32. 23,957 Gas labels were correctly

classified, as well as 23,768 Gas and Oil labels, 27438 Low-volume hydrocarbon labels, and 25,411 Oil labels were correctly classified.

Table 4.29. Random Forest hydrocarbon classification training dataset report

	Precision	Recall	F1-score	support
Gas	1.00	1.00	1.00	83986
Gas and Oil	1.00	1.00	1.00	84010
Low-volume Hydrocarbons	1.00	1.00	1.00	84000
Oil	1.00	1.00	1.00	84004
Accuracy			0.9999	336000

Table 4.30. Random Forest hydrocarbon classification validation dataset report

	Precision	Recall	F1-score	support
Gas	0.86	0.87	0.87	27378
Gas and Oil	0.85	0.86	0.85	27821
Low-volume Hydrocarbons	0.98	0.96	0.97	28533
Oil	0.91	0.90	0.90	28268
Accuracy			0.8962	112000

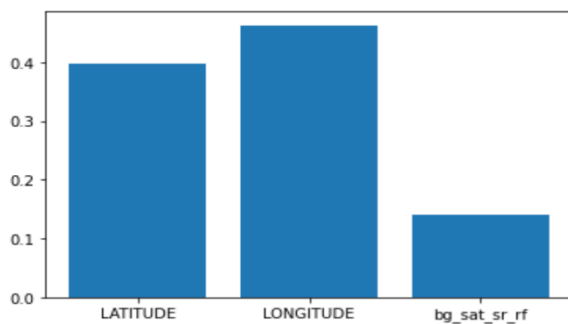
Table 4.31. Random Forest hydrocarbon classification testing report

	Precision	Recall	F1-score	support
Gas	0.86	0.87	0.86	27515
Gas and Oil	0.85	0.86	0.85	27669
Low-volume Hydrocarbons	0.98	0.96	0.97	28544
Oil	0.91	0.90	0.90	28272
Accuracy			0.8970	112000

Table 4.32. Classification confusion matrix for test dataset

Class	Gas	Gas and Oil	Low-volume Hydrocarbons	Oil
Gas	23957	2168	169	1221
Gas and Oil	2265	23768	346	1290
Low-volume Hydrocarbons	438	590	27438	78
Oil	1340	1474	47	25411

Figure 4.8 depicts the model input feature importance for the latitude, longitude, and Bouguer gravity values.



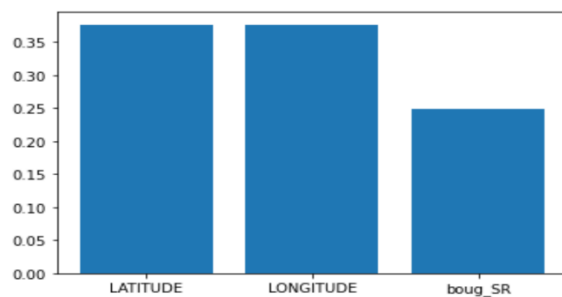
Input features	Feature Importance Score
Bouguer gravity	0.13935
Latitude	0.39817
Longitude	0.46248

Figure 4.8. Random Forest classification model feature importance

In the next approach, the Bouguer gravity interpolated using Petrel convergent algorithm, along with the latitude and longitude values were used as input features, while the output classes were oil, gas, oil and gas, and low-volume hydrocarbons. Table 4.23 shows the hydrocarbon classification results from using Petrel's interpolated Bouguer gravity data to account for its geospatial trend and the input feature importance is shown in Figure 4.9.

Table 4.33. Petrel hydrocarbon classification testing dataset report

	Precision	Recall	F1-score	support
Gas	0.88	0.85	0.86	33221
Gas and Oil	0.85	0.86	0.85	27355
Low-volume Hydrocarbons	0.96	0.97	0.96	25501
Oil	0.90	0.91	0.91	25923
Accuracy			0.8972	112000



Input features	Feature Importance Score
Bouguer gravity	0.24822
Latitude	0.37556
Longitude	0.37622

Figure 4.9. Petrel hydrocarbon classification model features importance

The third approach involved using the oil/gas field's Bouguer gravity, and free-air gravity values (interpolated using Random Forest regression) as input features, without including the

latitude and longitude coordinates as inputs. The output classes evaluated are hydrocarbon versus no hydrocarbons, oil versus no oil, and gas versus no gas. The classification input data used a train/test split ratio of 80/20. Tables 4.34 to 4.36, summarizes the comparison of the classification model's resulting performance using its F1-score accuracy values.

Table 4.34. Super resolution satellite-based hydrocarbons vs no hydrocarbons classification results

Super Resolution - Hydrocarbons vs No Hydrocarbons (HC vs nHC)										
		Train set F1-score accuracy			Test set F1-score accuracy			Blind test set F1-score accuracy		
Model		Random Forest			Random Forest			Random Forest		
Input features		Overall	HC	nHC	Overall	HC	nHC	Overall	HC	nHC
Train/test split ratio: 80/20	Bouguer gravity	94%	94%	94%	69%	69%	70%	66%	72%	57%
	Bouguer & free-air gravity	100%	100%	100%	88%	88%	88%	67%	73%	56%

Table 4.35. Super resolution satellite-based oil vs no oil classification training results

Super Resolution - Oil vs No Oil (O vs nO)										
		Train set F1-score accuracy			Test set F1-score accuracy			Blind test set F1-score accuracy		
Model		Random Forest			Random Forest			Random Forest		
Input features		Overall	O	nO	Overall	O	nO	Overall	O	nO
Train/test split ratio: 80/20	Bouguer gravity	96%	96%	96%	66%	66%	67%	51%	56%	45%
	Bouguer & free-air gravity	100%	100%	100%	84%	84%	84%	55%	63%	44%

Table 4.36. Super resolution satellite-based gas vs no gas classification training results

Super Resolution - Gas vs No Gas (G vs nG)									
		Train set F1-score accuracy			Test set F1-score accuracy			Blind test set F1-score accuracy	
Model		Random Forest			Random Forest			Random Forest	
Input features		Overall	G	nG	Overall	G	nG	Overall	G nG
Train/test split ratio: 80/20	Bouguer gravity	94%	94%	94%	62%	62%	62%	49%	48% 50%
	Bouguer & free-air gravity	100%	100%	100%	79%	79%	79%	47%	25% 59%

The results show that the trained model for different input features, the hydrocarbon vs no hydrocarbon had an average F1-score accuracy of 91.75% on the training dataset and roughly an average of 78% on the test dataset and roughly an average of 50% on the blind test dataset. For oil vs no oil classification, the results show that the trained model had an average F1-score accuracy of 92% on the training dataset and roughly an average of 74.25% on the test dataset and roughly an average of 53.25% on the blind test dataset. Lastly, for gas vs no gas classification, the results show that the trained model had an average F1-score accuracy of 90.25% on the training dataset and roughly an average of 74% on the test dataset and roughly an average of 49% on the blind test dataset. Similar to the land-based and satellite data models, the prediction for hydrocarbon versus no hydrocarbon was the best among the class combinations tested. The results for the blind testing at a different geographical location are not as robust, indicating the need for including additional input features for hydrocarbon prediction at a new location.

Chapter 5. CONCLUSION

This study shows the successful application of machine learning on gravity data for hydrocarbon classification (into gas, oil, and low hydrocarbon regions). The Random Forest regression model provides adequate geospatial trend for the interpolation of the gravity data with good accuracy. Deep learning based super-resolution offers a robust approach to improve the low spatial resolution and precision of satellite-based gravity data. The modeling results indicate that both the land-based and satellite-based gravity anomaly enhanced through super-resolution give similar hydrocarbon classification performance and interpolation accuracy. The prediction accuracy improves by including latitude and longitude information at the well and field locations as input feature, although results are good even when only Bouguer and isostatic gravity anomalies are used as inputs. Among the different class combinations evaluated, prediction of hydrocarbon versus no hydrocarbon was most accurate in land-based, satellite, and enhanced-satellite data cases. The prediction accuracy for blind test set (at a separate geographical location) was in general low, indicating the need for additional input features for mapping gravity to hydrocarbon deposits in new areas. The results from unsupervised machine learning approach, Self-Organizing Map (SOM), generated low accuracy as compared to the Random Forest model, indicating that a supervised machine learning is more suitable for predicting hydrocarbon locations when only the gravity information is available. This study demonstrates that the machine learning-assisted workflow utilizing gravity anomalies (from land-based or satellite measurements) has the potential to be used as an early screening tool that provides a cost-effective, quick, and computationally efficient approach for hydrocarbon exploration.

Chapter 6. RECOMMENDATIONS

The hydrocarbon classification in this study was performed using Bouguer gravity, isostatic gravity, latitude, and longitude coordinates. However, the density distribution in the Earth's interior can be determined with improved accuracy by directly measuring the spatial derivatives of the gravity vector (Condi & Talwani, 1999; Fairhead, 2016). Although several parameters have been investigated in this study, other parameters that could improve the robustness of the machine learning model outside of these parameters still exist. For instance, gravity gradiometry which measures the variations in the acceleration due to gravity has predominantly been used to image subsurface geology as a valid support for hydrocarbon and mineral exploration. The most frequently used and intuitive component is the vertical gravity gradient, G_{zz} , which represents the rate of change of vertical gravity with depth (z). Future work can also include model training with more data from the US as well as other countries and machine learning model architecture improvements. Since the main objective of this work was to develop a quick screening tool, more rigorous and extensive exploration studies could also incorporate geological parameters obtained from seismic acquisition, well logging, and other geophysical techniques. Such parameters could include formation resistivity values, fluid contacts, existence of faults, fractures, sedimentary thickness, and others.

BIBLIOGRAPHY

- Adelman, M. A. (1970). Economics of exploration for petroleum and other minerals. *Geoexploration*, 8(3–4), 131–150. [https://doi.org/10.1016/0016-7142\(70\)90030-X](https://doi.org/10.1016/0016-7142(70)90030-X)
- Aghajani, H., Moradzadeh, A., & Zeng, H. (2011). Detection of high-potential oil and gas fields using normalized full gradient of gravity anomalies: A case study in the Tabas basin, eastern Iran. *Pure and Applied Geophysics*, 168(10), 1851–1863. <https://doi.org/10.1007/s00024-010-0169-y>
- Airy, G. B. (1855). On the computation of the effect of the attraction of the mountain-masses, as disturbing the apparent astronomical latitude of stations in geodetic surveys. *Royal Society of London, Philosophical Transactions*, 145, 101–104.
- Baker, S., & Kanade, T. (2002). Limits on super-resolution and how to break them. *IEEE Transactions on Pattern Analysis and Machine Intelligence*, 24(9), 1167–1183. <https://doi.org/10.1109/TPAMI.2002.1033210>
- Chen, J., Schiek-Stewart, C., Lu, L., Witte, S., Guardia, K. E., Menapace, F., Devarakota, P., & Sidahmed, M. (2020). Machine learning method to determine salt structures from gravity data. *Proceedings - SPE Annual Technical Conference and Exhibition, 2020-October*(Seaborne 2002). <https://doi.org/10.2118/0221-0070-jpt>
- Condi, F., & Talwani, M. (1999). Resolution and efficient inversion of gravity gradiometry. *1999 SEG Annual Meeting*, 358–361. <https://doi.org/10.1190/1.1821022>
- Crowley, J. W., Mitrovica, J. X., Bailey, R. C., Tamisiea, M. E., & Davis, J. L. (2006). Land water storage within the Congo Basin inferred from GRACE satellite gravity data. *Geophysical Research Letters*, 33(19), 2–5. <https://doi.org/10.1029/2006GL027070>
- Dong, C., Loy, C. C., He, K., & Tang, X. (2015). Image super-resolution using deep convolutional networks. *IEEE Transactions on Pattern Analysis and Machine Intelligence*, 38(2), 295--307.
- Dong, C., Loy, C. C., He, K., & Tang, X. (2014). Learning a deep convolutional network for image super-resolution. *European Conference on Computer Vision*, 184--199.
- Fairhead, D. (2016). Advances in Gravity and Magnetic Processing and Interpretation. *Advances in Gravity and Magnetic Processing and Interpretation*, 352. <https://doi.org/10.3997/9789462821750>
- Kern, M., Schwarz, K. P., & Sneeuw, N. (2003). A study on the combination of satellite, airborne, and terrestrial gravity data. *Journal of Geodesy*, 77(3), 217–225. <https://doi.org/10.1007/s00190-003-0313-x>
- Shiloh-Perl, L., & Giryes, R. (2020). Introduction to deep learning. *ArXiv, Dli*. https://doi.org/10.1007/978-1-4842-5177-5_3

- Sokolov, A. V. (2011). High accuracy airborne gravity measurements. Methods and equipment. *IFAC Proceedings Volumes (IFAC-PapersOnline)*, 44(1 PART 1), 1889–1891. <https://doi.org/10.3182/20110828-6-IT-1002.01892>
- Zhang, Yi; Xin (Shane) Li; Sharma, J. (2021). *Deep Learning Based Super Resolution of Gravity Data for Geophysical Exploration*. Louisiana State University.
- Babakhani, M. (2018). Uncertainty Analysis in Geological Surface Modelling (Duvernay Formation / Muskwa Formation and Leduc Formation Case Studies). *Alberta Geological Survey*.
- Balmino, G., & Bonvalot, S. (2016). *Encyclopedia of Geodesy*. <https://doi.org/10.1007/978-3-319-02370-0>
- Balmino, G., Vales, N., Bonvalot, S., and Briais, A. (2012). Spherical harmonic modelling to ultra-high degree of Bouguer and isostatic anomalies. *Journal of Geodesy*, 86, 499–520. <https://doi.org/10.1007/s00190-011-0533-4>
- BEREZKIN, V. M. (n.d.). *Application of gravity exploration to reconnaissance of oil*.
- Breiman, L. (1996). *Bagging predictors*. *Machine learning*, 123–140.
- Breiman, L. (2001). *Random Forests*. *Machine learning*. 45(1), 5–32.
- Cutler, D. R., Edwards, T. C., Beard, K. H., Cutler, A., Hess, K. T., Gibson, J., & Lawler, J. J. (2007). Random Forests for classification in ecology. *Ecology*, 88(11), 2783–2792. <https://doi.org/10.1890/07-0539.1>
- De Castro D L and Bezerra F H R. (2011). Castelo branco. *J. South American Earth Sci*, 26(3).
- Dietterich, T. G. (2000). Experimental comparison of three methods for constructing ensembles of decision trees: bagging, boosting, and randomization. *Machine Learning*, 40(2), 139–157. <https://doi.org/10.1023/A:1007607513941>
- Dung, T. T. (2004). Two- and three-dimensional normalized total gradient of gravity anomalies and its application for detecting the oil-gas potential areas in the southeast sedimentary basins of the East Vietnam Sea. *7th SEGJ Int Symp Imag Technol, Sendai, Japan*.
- Ervin, C. P. (1977). Theory of the Bouguer Anomaly. *Geophysics*, 42(7), 1468–1468. <https://doi.org/10.1190/1.1440807>
- Fayad, I., Baghdadi, N., Bailly, J. S., Barbier, N., Gond, V., Hérault, B., El Hajj, M., Fabre, F., & Perrin, J. (2016). Regional scale rain-forest height mapping using regression-kriging of spaceborne and airborne LiDAR data: Application on French Guiana. *Remote Sensing*, 8(3). <https://doi.org/10.3390/rs8030240>

- Fouedjio, F. (2020). Exact Conditioning of Regression Random Forest for Spatial Prediction. *Artificial Intelligence in Geosciences*, 1(January), 11–23. <https://doi.org/10.1016/j.aiig.2021.01.001>
- Gunnarsson, N. (2011). 3D modeling in Petrel of geological CO₂ storage site. *Examensarbete 30 Hp*, November, 52.
- Hengl, T., Heuvelink, G. B. M., Kempen, B., Leenaars, J. G. B., Walsh, M. G., Shepherd, K. D., Sila, A., MacMillan, R. A., De Jesus, J. M., Tamene, L., & Tondoh, J. E. (2015). Mapping soil properties of Africa at 250 m resolution: Random Forests significantly improve current predictions. *PLoS ONE*, 10(6). <https://doi.org/10.1371/journal.pone.0125814>
- Hengl, T., Nussbaum, M., Wright, M. N., Heuvelink, G. B. M., & Gräler, B. (2018). Random Forest as a generic framework for predictive modeling of spatial and spatio-temporal variables. *PeerJ*, 2018(8). <https://doi.org/10.7717/peerj.5518>
- Heywood, C. (1992). Isostatic Residual Gravity Anomalies of New Mexico. *Usgs*. <https://doi.org/19.42/4:91.4065>
- Karl, J. H. (1971). the Bouguer Correction for the Spherical Earth. *Geophysics*, 36(4), 761–762. <https://doi.org/10.1190/1.1440211>
- Kearey, P., & Brooks, M. (1991). An introduction to geophysical exploration. 2nd edition. *An Introduction to Geophysical Exploration. 2nd Edition*, 40(1), 24.
- Keller, C. P. (1995). Geographic information systems for geoscientists: Modelling with GIS. *Computers & Geosciences*, 21(9), 1110–1112. [https://doi.org/10.1016/0098-3004\(95\)90019-5](https://doi.org/10.1016/0098-3004(95)90019-5)
- Kirkwood, C., Cave, M., Beamish, D., Grebby, S., & Ferreira, A. (2016). A machine learning approach to geochemical mapping. *Journal of Geochemical Exploration*, 167, 49–61. <https://doi.org/10.1016/j.gexplo.2016.05.003>
- Kucks, R. P. (1999). Bouguer gravity anomaly data grid for the conterminous US. *Bouguer Gravity Anomaly Data Grid for the Conterminous US*.
- Liu, G., Scott, R., & O'Halloran, G. (2020). Gravity and magnetic data applications for hydrocarbon exploration offshore NW Australia. *SEG International Exposition and Annual Meeting 2019*, 1695–1698. <https://doi.org/10.1190/segam2019-3196255.1>
- Liu, L., Zhang, M., Wang, P., Zhang, S., Qiao, J., Yu, H., & Huang, J. (2018). Construction of geophysical-geological structural models for complex basins: Application of interpretation of gravity, magnetic, electric, and seismic data to exploration in the Chuxiong basin. *Acta Geophysica Sinica*, 61(12), 4921–4933. <https://doi.org/10.6038/cjg2018L0718>
- Lowrie, W. (1997). Fundamentals of Geophysics, Cambridge University Press. *New York, USA*.

- McCulloh, T. H. (1967). Mass Properties of Sedimentary Rocks and Gravimetric Effects of Petroleum and Natural-Gas Reservoirs. *Geological Survey Professional Paper*, 528-A.
- Mclay, A. K., Muggli, R., & Mazrui, S. (2003). ArcGIS in the Oil and Gas Exploration Workflow Petroleum Development Oman. *23rd Annual ESRI International User Conference San Diego*.
- McLean, M. A., Wilson, C. J. L., Boger, S. D., Betts, P. G., Rawling, T. J., & Damaske, D. (2009). Basement interpretations from airborne magnetic and gravity data over the Lambert rift region of east Antarctica. *Journal of Geophysical Research: Solid Earth*, 114(6). <https://doi.org/10.1029/2008JB005650>
- P. Hill, V. Bankey, Vi. L. (1997). Introduction to Potential Fields: Gravity. *Usgs*, 239(95), 1–2.
- Pedregosa, F. and Varoquaux, G., Gramfort, A. and Michel, V., Thirion, B. and Grisel, O., Blondel, M. and Prettenhofer, P., Weiss, R. and Dubourg, V., Vanderplas, J. and Passos, A., Cournapeau, D. and Brucher, M., Perrot, M., & Duchesnay, E. (2011). Scikit-learn: Machine Learning in {P}ython. *Journal of Machine Learning Research*, 12, 2825–2830.
- Pratt, J. H. (1855). On the attraction of the Himalaya Mountains, and of the elevated regions beyond them upon the plumbline in India. *Royal Society London, Philosophical Transactions*, 145, 53–100.
- R. Shapire, Y. Freund, P. Bartlett, and W. L. (1998). Boosting the margin: A new explanation for the effectiveness of voting methods. *Annals of Statistics*, 26(5), 1651–1686.
- Ruppert, D. (2004). The Elements of Statistical Learning: Data Mining, Inference, and Prediction. *Journal of the American Statistical Association*, 99(466), 567–567. <https://doi.org/10.1198/jasa.2004.s339>
- Sarsar Naouali, B., Guellala, R., Bey, S., & Inoubli, M. H. (2017). Gravity Data Contribution for Petroleum Exploration Domain: Mateur Case Study (Saliferous Province, Northern Tunisia). *Arabian Journal for Science and Engineering*, 42(1), 339–352. <https://doi.org/10.1007/s13369-016-2152-0>
- Srinivasan, B. V., Duraiswami, R., & Murtugudde, R. (2008). Efficient Kriging for Real-Time Spatio-Temporal Interpolation. *20Th Conference on Probability and Statistics in Atmospheric Sciences*, 228–235.
- Szatmári, G., & Pásztor, L. (2019). Comparison of various uncertainty modelling approaches based on geostatistics and machine learning algorithms. *Geoderma*, 337, 1329–1340. <https://doi.org/10.1016/j.geoderma.2018.09.008>
- Takin, M., & Talwani, M. (1966). Rapid Computation of the Gravitation Attraction of Topography on a Spherical Earth. *Geophysical Prospecting*, 14(2), 119–142. <https://doi.org/10.1111/j.1365-2478.1966.tb01750.x>

- Vaysse, K., & Lagacherie, P. (2017). Using quantile regression forest to estimate uncertainty of digital soil mapping products. *Geoderma*, 291, 55–64. <https://doi.org/10.1016/j.geoderma.2016.12.017>
- Veronesi, F., & Schillaci, C. (2019). Comparison between geostatistical and machine learning models as predictors of topsoil organic carbon with a focus on local uncertainty estimation. *Ecological Indicators*, 101, 1032–1044. <https://doi.org/10.1016/j.ecolind.2019.02.026>
- Yanis, M., & Marwan. (2019a). The potential use of satellite gravity data for oil prospecting in Tanimbar Basin, Eastern Indonesia. *IOP Conference Series: Earth and Environmental Science*, 364(1). <https://doi.org/10.1088/1755-1315/364/1/012032>
- Yanis, M., & Marwan. (2019b). The potential use of satellite gravity data for oil prospecting in Tanimbar Basin, Eastern Indonesia. *IOP Conference Series: Earth and Environmental Science*, 364(1). <https://doi.org/10.1088/1755-1315/364/1/012032>
- Zamora, A. (2013). *On Different Techniques for The Calculation of Bouguer Gravity Anomalies for Joint Inversion and Model Fusion of Geophysical Data In The Rio Grande Rift Program in Computational Science*.
- Zhang, M. H., Qiao, J. H., Tian, Q. N., Liu, L., Gao, F., & Sun, Z. R. (2013). Gravity and magnetic anomaly interpretation for oil and gas basins in Southeast Daxingan Mountains. *Geological Bulletin of China*, 32(8), 1177–1184.
- Zhang, M. hua, Qiao, J. hua, Zhao, G. xin, & Lan, X. yi. (2019). Regional gravity survey and application in oil and gas exploration in China. *China Geology*, 2(3), 382–390. [https://doi.org/10.1016/S2096-5192\(19\)30188-0](https://doi.org/10.1016/S2096-5192(19)30188-0)

VITA

Oluwafemi T. Alaofin graduated from Nigeria's Ladoke Akintola University of Technology with a bachelor's degree in chemical engineering. He previously interned as an upper well completion intern at Schlumberger Oilfield Services. Following that, he earned a master's degree in subsea engineering from the Offshore Technology Institute at the University of Port Harcourt in Rivers, Nigeria. In 2018, he enrolled at Louisiana State University to pursue a master's degree in petroleum engineering. He plans to graduate with a master's degree in petroleum engineering and a minor in computer science in the spring of 2022. He previously interned as a data science intern at Snap Inc. He has accepted a position as an engineering data scientist at Snap Inc. in Santa Monica, California, beginning in the spring of 2022.